DYNAMICS AND CONTROL OF A PLANAR TENSEGRITY ROBOT ARM

A Thesis

by

ARITRA BISWAS

Submitted to the Office of Graduate and Professional Studies of
Texas A&M University
in partial fulfillment of the requirements for the degree of

MASTER OF SCIENCE

Chair of Committee,	Raktim Bhattacharya
Co-Chair of Committee,	Robert Skelton
Committee Member,	Pilwon Hur
Head of Department,	Rodney Bowersox

December 2017

Major Subject: Aerospace Engineering

ABSTRACT

Tensegrity structures have been used in the field of engineering and architecture over the last half century to build static load-bearing structures. These structures are built out of a network of rigid bars and elastic strings which are connected to each other at their ends. The primary advantage of these structures is that the elements are under axial loading only which dramatically reduces their minimal mass.

Recently tensegrity structures have gained interest in the Space community which is in need of lightweight robot designs for planetary exploration and spacecraft maintenance. This research work aims to address some of the challenges in tensegrity research. Firstly, this work presents minimal mass design of a planar tensegrity robot arm and compares with a conventional design. Then the robot's dynamics is formulated using Lagrange's method. Finally, optimal control theory is utilized to solve two control problems - stabilization in the presence of disturbance and noise and robust tracking of a desirable trajectory.

DEDICATION

To my parents, whose love and support brought me this far.

ACKNOWLEDGMENTS

I owe my sincere thanks to my advisors Dr. Raktim Bhattacharya, Dr. Robert Skelton and Dr. Pilwon Hur for their guidance and control during my term as a graduate student. I am also grateful to my colleagues at the Uncertainity Quantification Laboratory, Texas A&M University for participating in regular academic discussions.

CONTRIBUTORS AND FUNDING SOURCES

Contributors

This work was supported by a thesis committee consisting of Professor Raktim Bhattacharya and Professor Robert Skelton of the Department of Aerospace Engineering and Professor Pilwon Hur of the Department of Mechanical Engineering.

All work for the thesis was completed by the student, under the advisement of the thesis committee comprising of Professor(s) Bhattacharya, Skelton and Hur.

Funding Sources

This work was funded by NASA NIAC Phase II Grant on Tensegrity Approaches to In-Space Construction of a 1g Growable Habitat.

TABLE OF CONTENTS

Page

LIST OF FIGURES

FIGURE Page

LIST OF TABLES

TABLE Page

1. INTRODUCTION AND LITERATURE REVIEW

1.1 Motivation

The term Tensegrity was coined by Buckminster Fuller from *tension* and *integrity*, symbolizing that such structures acquire stability through tensile forces in its members. Tensegrity structures have been used in the field of engineering and architecture over the last half century to build static load-bearing structures. They are built out of a network of bars and strings which are connected to each other at their ends. These structures have compressive as well as tensile parts - the compressive loads are taken by the bars whereas the tensile loads are taken by strings or cables.

Recently, Tensegrity has achieved interest in the space community because of the lightweight design capabilities and this research work is a step towards that direction. This work concentrates on designing and building a tensegrity inspired robotic arm that can perform manipulation tasks of an actual robotic arm. The scope of this work is limited to planar motion of the manipulator only and serves as a conceptual proof that tensegrity robotics can be implemented as a viable solution for space applications.

1.1.1 Literature Review

Much work has been done on the geometry and form finding of tensegrity structures along with the development of tensegrity dynamics in non-minimal coordinates which greatly simplifies the dynamics equations. However, this research work uses minimal coordinates to develop the dynamics and is later elaborated.

Early works on tensegrity structures are attributed to Fuller [2] whose work provides much foundation to the static stability of these structures. Further examples of understanding equilibrium of rods and strings are found in the works of Pellegrino

[3] and Guest [4]. Nagase and Skelton [5] presents a framework for minimal mass design of tensegrity structures which shows that structural mass is greatly reduced by avoiding material bending. However, there was little interest in the dynamics of tensegrity structures much due to their complexity. Cheong and Skelton [6] presents tensegrity dynamics in a new light by using non-minimal coordinates. This is one of the simplest forms of the dynamics equations which have a matrix structure, constant inertia matrix and no trigonometric functions. The optimal control theory formulations used in this text have been derived from the work of Doyle et. al. [7].

1.1.2 Research Objectives

The objective of this research work is to design and build a planar tensegrity robot arm and can be classified into the following high level tasks.

1. Demonstration of mass minimization
2. Modeling of the dynamics
3. Stabilization using string actuation
4. Trajectory tracking

It is useful to define some key tensegrity concepts which are elaborated in the following sections. These concepts form the basis for most tensegrity discussions in the upcoming sections.

1.2 Form Finding

A key step in the design of tensegrity structures is the determination of their geometrical configuration, known as form-finding. Matrix algebra can be used to develop the geometry and form of tensegrity structures.

1.2.1 Nodes, Bars and Strings

Let the given structure be composed of β **bars** and η **strings**. It is important that the strings and bars be connected to each other at their ends only, this eliminates non-axial loading such as bending, shear and torsion. The ends of the bars are termed as **nodes**, and when the bars are connected at their ends the nodes overlap. Additionally, nodes can be purely connected to strings.

The bars will be marked in black, strings in red and nodes as circles and this will be the nomenclature that will be followed in this work.

1.2.2 Node Matrix

A static tensegrity system in Cartesian coordinates can be expressed by a node matrix $\mathbf{N} \in \mathbb{R}^{3\times n}$ where n is the total number of nodes in the system.

$$\mathbf{N} = [\mathbf{n_1} \quad \mathbf{n_2} \quad ... \quad \mathbf{n_n}]_{3\times n} \tag{1.1}$$

where $\mathbf{n_1}, \mathbf{n_2}, ..., \mathbf{n_n}$ are the vectors that represent the nodes of the system.
It is important to establish the connectivity of the bars and strings with respect to the nodes in a meaningful way. A matrix consisting of 1s, -1s and 0s can be utilized to express the connectivities. This matrix is called the **connectivity matrix**.

1.2.3 Bar Connectivity

The connectivity of bars with respect to the nodes can be expressed by the bar connectivity matrix $\mathbf{C_b} \in \mathbb{R}^{\beta \times n}$. The i, j^{th} element of this matrix is given by

$$c_b^{i,j} = \begin{cases} -1 & \text{if bar } i \text{ starts at node } j \\ 1 & \text{if bar } i \text{ ends at node } j \\ 0 & \text{if there is no connectivity} \end{cases}$$

Consequently, the matrix representing the bar vectors can be expressed as

$$\mathbf{B} = \mathbf{N}\mathbf{C}_\mathbf{b}^\mathbf{T} \tag{1.2}$$

Now, each column of the matrix $\mathbf{B} \in \mathbb{R}^{3 \times \beta}$ represents a bar vector.

1.2.4 String Connectivity

The connectivity of strings with respect to the nodes can be expressed in a similar fashion through the string connectivity matrix $\mathbf{C_s} \in \mathbb{R}^{\eta \times n}$.

$$c_s^{i,j} = \begin{cases} -1 & \text{if string } i \text{ starts at node } j \\ 1 & \text{if string } i \text{ ends at node } j \\ 0 & \text{if there is no connectivity} \end{cases}$$

The matrix representing the string vectors can be expressed as

$$\mathbf{S} = \mathbf{N}\mathbf{C}_\mathbf{s}^\mathbf{T} \tag{1.3}$$

Each column of the matrix $\mathbf{S} \in \mathbb{R}^{3 \times \eta}$ represents a string vector.

1.2.5 Force Densities and Equilibrium

Static equilibrium of a mechanical system is defined as the state in which all externally applied forces and moments equal to the internal forces. In tensegrity systems, external forces are those that are acting on the nodes and internal forces are the forces in the bars and strings.

In order to solve complex nonlinear equilibrium equations in a simpler way, the concept of force density is introduced. The force density in each member of the tensegrity system may be defined as the ratio of the scalar magnitude of forces acting on that member to the length of that member. The force densities are denoted by λ_i for bars and γ_i for strings.

Defining the bar and string force density matrices as,

$$\mathbf{\Lambda}_{\beta\times\beta} = \begin{bmatrix} \lambda_1 & ... & 0 \\ \vdots & \lambda_2 & \vdots \\ 0 & ... & \lambda_\beta \end{bmatrix}$$

$$\mathbf{\Gamma}_{\eta\times\eta} = \begin{bmatrix} \gamma_1 & ... & 0 \\ \vdots & \gamma_2 & \vdots \\ 0 & ... & \gamma_\eta \end{bmatrix}$$

where

$$\lambda_i = \frac{f_i^{bar}}{||\mathbf{b_i}||}, \quad \gamma_i = \frac{f_i^{string}}{||\mathbf{s_i}||}$$

Let $\mathbf{W} \in \mathbb{R}^{3\times n}$ be the matrix of externally applied forces at the nodes and $\mathbf{W_r} \in \mathbb{R}^{3\times n}$ be the reaction forces at the pinned nodes. Recall that in order to enable pure tension or compression in the members, external forces are assumed to

act at the nodes only. Then the equilibrium of forces [1] is given by

$$\begin{bmatrix} \mathbf{B} & \mathbf{S} \end{bmatrix} \begin{bmatrix} -\mathbf{\Lambda} & \mathbf{0} \\ \mathbf{0} & \mathbf{\Gamma} \end{bmatrix} \begin{bmatrix} \mathbf{C_b} \\ \mathbf{C_s} \end{bmatrix} = \mathbf{W} + \mathbf{W_r} \tag{1.4}$$

which is linear in $\mathbf{\Lambda}$ and $\mathbf{\Gamma}$. Often, this will lead to an undetermined system of linear equations and can be solved by any optimization algorithm. By convention, bar forces are compressive and will be negative whereas string forces are tensile and positive. Additionally the constraints $\mathbf{\Lambda} \geq \mathbf{0}, \mathbf{\Gamma} \geq \mathbf{0}$ must be enforced, note that negative sign in $\mathbf{\Lambda}$ denotes compression. Eq. (1.4) will be used throughout this text to calculate the equilibrium forces and will be useful during linearization of the dynamics.

2. DESIGN OF TENSEGRITY ROBOT ARM

2.1 Material Selection

One high level objective for this research work is to make the tensegrity robot arm lighter than a traditional robot arm. Mass minimization is achieved in tensegrity systems by the elimination of non-axial loads. The axial member loads are compression in bars and tension in strings. Assuming that the bars are built out of isotropic material (eg. metals such as Aluminum and Steel) it can be safely said that buckling shall occur sooner than material yielding by compression. Hence the bars are designed to withstand buckling. For strings, choice of material is made such that failure will occur due to material yielding by tension and strings will obey *Hooke's Law of Elasticity*.

2.2 Minimal Mass Tensegrity Structures

The tensegrity robot arm will be built from smaller tensegrity systems (also called building blocks) which are **self-similar**. The two major building blocks used in this design are **T-Bars** and **D-Bars**. The notion of *self-similarity* implies that a geometrical structure can be replaced by another geometrical structure of similar behavior in an iterative process. Since metals are more mass-efficient in tension than compression, the goal will be to minimize the usage of compressive members (bars) and replace them with tensile members (strings). In our analysis we assume that string masses will be negligible as compared to bar masses.

2.2.1 T-Bar

A T-Bar is a self similar tensegrity system that is comprised of 4 rigid bars (black) and 4 strings (red) connected in a fashion shown in Fig. 2.1. Consider that

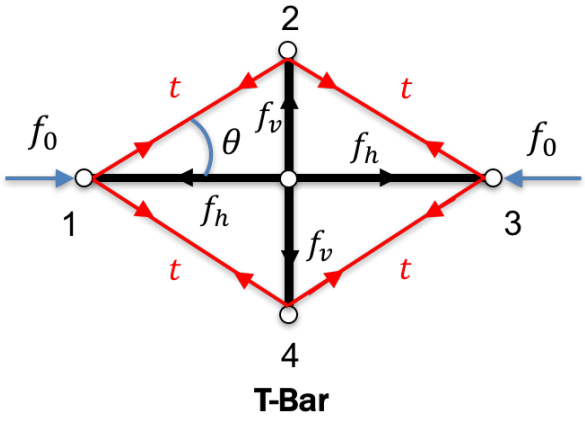

Figure 2.1: A unit T-Bar

the robot has to withstand compressive loads, then the most simple solution is a column designed to withstand buckling. Now, the goal is to replace this column by a tensegrity structure (in this case a T-Bar) and it is important to compare the minimal masses in each case.

For a slender column with length l_0 and radius r_0, the critical buckling load f_0 is given by Euler's equation

$$f_0 = \frac{\pi^2 EI}{l_0^2}$$

where $I = \frac{\pi r_0^4}{4}$ is the polar moment of inertia of the column and E_b is the modulus of elasticity. The minimal mass for this column is given by

$$m_0 = 2\rho_b \sqrt{\frac{f_0}{\pi E_b}} l_0^2 \tag{2.1}$$

where $\rho_b = \frac{m_0}{\pi r_0^2 l_0}$ is the density of the column material.

It is shown in [1] that the T-Bar is a minimal mass design for a compressive load. The T-Bar's mass can be computed by analyzing the member forces in the loaded and unloaded case. Consider a T-Bar with the same horizontal length l_0 as

the column. The horizontal and vertical bars are of length l_h and l_v with compressive forces f_h and f_v respectively. Each of the 4 strings have length s and tension t. In the loaded case, only the horizontal bars are loaded and the tension t is zero. The equilibrium equations are given by

$$t = 0 \tag{2.2}$$

$$f_h = 2t\cos\theta + f_0 = f_0 \tag{2.3}$$

$$f_v = 2t\sin\theta = 0 \tag{2.4}$$

In the unloaded case, there is no external force and the tension t should stabilize the system. If we choose the tension t such that it creates the same load f_0 in the horizontal bars as in the loaded case, then

$$t = \frac{f_h}{2\cos\theta} = \frac{f_0}{2\cos\theta} \tag{2.5}$$

$$f_v = 2t\sin\theta = f_0\tan\theta \tag{2.6}$$

The minimum mass of the bars will be the maximum of the masses obtained from the loaded and unloaded case. Since these are compressive forces we can subject the failure of the bars to the buckling equation. In that case the mass of the horizontal bars are given by

$$m_h = 2\rho_b\sqrt{\frac{f_0}{\pi E_b}}\left(\frac{l_0}{2}\right)^2 \tag{2.7}$$

Since the load f_v is zero in the loaded case, the mass of the vertical bars will be

obtained from the unloaded case

$$m_v = 2\rho_b \sqrt{\frac{f_0 \tan\theta}{\pi E_b}} \left(\frac{l_0 \tan\theta}{2}\right)^2 \tag{2.8}$$

The strings will be designed on yield limit of the material and the yield stress σ in the string should be less than the allowable yield stress σ_s

$$\sigma = \frac{t}{A_s} \leq \sigma_s \tag{2.9}$$

The cross-sectional area of the string A_s can be written in terms of the mass m_s, string length s and density of string material ρ_s

$$A_s = \pi r_s^2 = \frac{m_s}{s\rho_s} \tag{2.10}$$

The length of the string can be obtained from the geometrical relationships of the T-Bar members ($s = \frac{l_0}{2\cos\theta}$) and the tension t can be obtained from the Eq. (2.5). In the limiting case of Eq. (2.9) the mass of each string is obtained as

$$m_s = \frac{\rho_s}{\sigma_s} st = \frac{\rho_s}{\sigma_s} \left(\frac{l_0}{2\cos\theta}\right) \left(\frac{f_0}{2\cos\theta}\right) \tag{2.11}$$

Hence the mass of the unit T-Bar system (we can call this a T-Bar system with complexity 1) can be given as

$$m_t = 2m_h + 2m_v + 4m_s \tag{2.12}$$

$$= \rho_b \sqrt{\frac{f_0}{\pi E_b}} l_0^2 \left(1 + \tan^{5/2}\theta\right) + \frac{\rho_s l_0 f_0}{\sigma_s} \left(1 + \tan^2\theta\right) \tag{2.13}$$

The ratio of the T-Bar mass m_t to the mass of the original column m_0 is

$$\mu_1 = \frac{m_t}{m_0} = \frac{1}{2}\left(1 + \tan^{5/2}\theta\right) + \epsilon\left(1 + \tan^2\theta\right) \tag{2.14}$$

where

$$\epsilon = \frac{\rho_s\sqrt{\pi E_b f_0}}{2\rho_b\sigma_s l_0}$$

is a dimensionless parameter. It can be seen that from Fig. 2.2 that $\mu_1 < 1$ when $\epsilon < 1/2$ which is the required condition for mass reduction. The upper bound on θ can be then calculated by selecting the value of ϵ and finding the angle for which $\mu_1 = 1$.

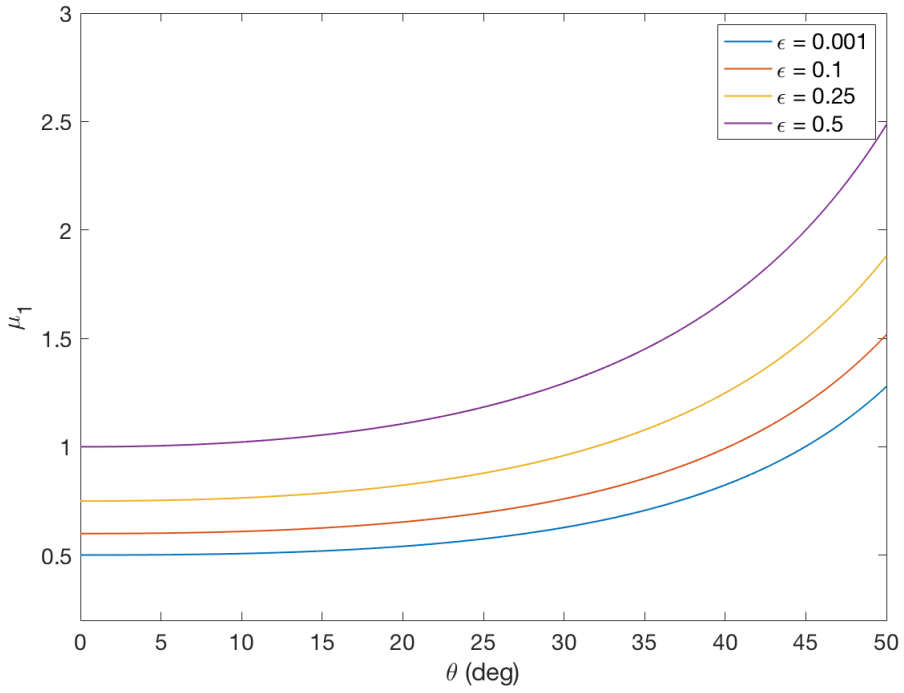

Figure 2.2: Mass reduction for a unit T-Bar [1]

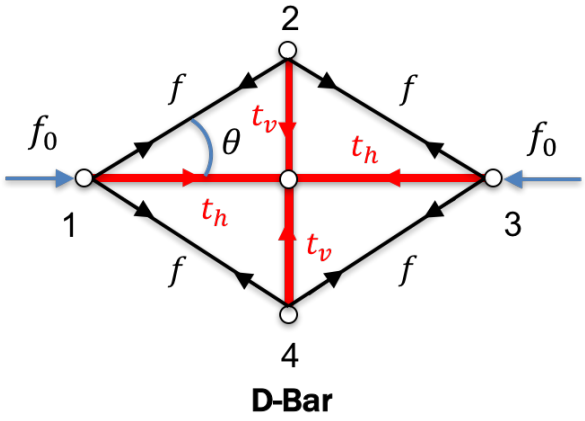

Figure 2.3: A unit D-Bar

2.2.2 D-Bar

If the bars in the unit T-Bar are replaced by strings and the strings by bars a unit D-Bar is obtained. In other words, a D-Bar is a geometrical inverse of a T-Bar as shown in Fig. 2.3. D-Bars are especially good for extensibility and retractability and are used in this design for the same purpose. The minimal mass of a D-Bar unit [1] is obtained as follows. Consider the D-Bar unit shown in Fig. In the loaded case the equilibrium equations are

$$t_h = 0 \tag{2.15}$$

$$f = \frac{f_0 + t_h}{2\cos\theta} = \frac{f_0}{2\cos\theta} \tag{2.16}$$

$$t_v = 2f\sin\theta = f_0\tan\theta \tag{2.17}$$

In the unloaded case, we choose the tensions t_v and t_h to stabilize the system such that the same load in Eq. (2.16) occurs in the bars. The equilibrium equations are

$$t_v = f_0 \tan\theta \tag{2.18}$$

$$t_h = 2f\cos\theta = f_0 \tag{2.19}$$

Similar to the T-Bar case, the minimum mass of each bar m is the maximum of the masses obtained from the loaded and unloaded cases. However, we have assumed that the bars are subject to the same load $f_0/2\cos\theta$ so

$$m = 2\rho_b\sqrt{\frac{f_0}{2\pi E_b\cos\theta}}\left(\frac{l_0}{2\cos\theta}\right)^2 \tag{2.20}$$

$$= \frac{1}{2}\rho_b l_0^2\sqrt{\frac{f_0}{\pi E_b}}\left(\frac{1}{2\cos\theta}\right)^{5/2} \tag{2.21}$$

Similar to Eq. (2.11) the mass of the horizontal string $m_{s,h}$ and vertical string $m_{s,v}$ are obtained by equating the tensile stress to the yield limit of the material.

$$m_{s,h} = \frac{\rho_s}{\sigma_s}s_h t_h = \frac{\rho_s}{\sigma_s}\left(\frac{l_0}{2}\right)(f_0) \tag{2.22}$$

$$m_{s,v} = \frac{\rho_s}{\sigma_s}s_v t_v = \frac{\rho_s}{\sigma_s}\left(\frac{l_0}{2}\tan\theta\right)(f_0\tan\theta) \tag{2.23}$$

The total mass of the D-Bar system is

$$m_d = 4m + 2m_{s,h} + 2m_{s,v} \tag{2.24}$$

$$= 2\rho_b l_0^2\sqrt{\frac{f_0}{\pi E_b}}\left(\frac{1}{2\cos\theta}\right)^{5/2} + \frac{\rho_s l_0 f_0}{\sigma_s}(1+\tan^2\theta) \tag{2.25}$$

and the ratio between the mass of the D-Bar to the mass of the original column is therefore

$$\mu_2 = \frac{m_d}{m_0} = \left(\frac{1}{2\cos\theta}\right)^{5/2} + \epsilon\left(1 + \tan^2\theta\right) \tag{2.26}$$

Fig. 2.4 shows the variation of μ_2 with θ for different values of ϵ. It can be noted that for $\epsilon = 0.2929$ the value of μ_2 was greater than or equal to 1 which necessitates that $\epsilon < 0.2929$ for mass reduction.

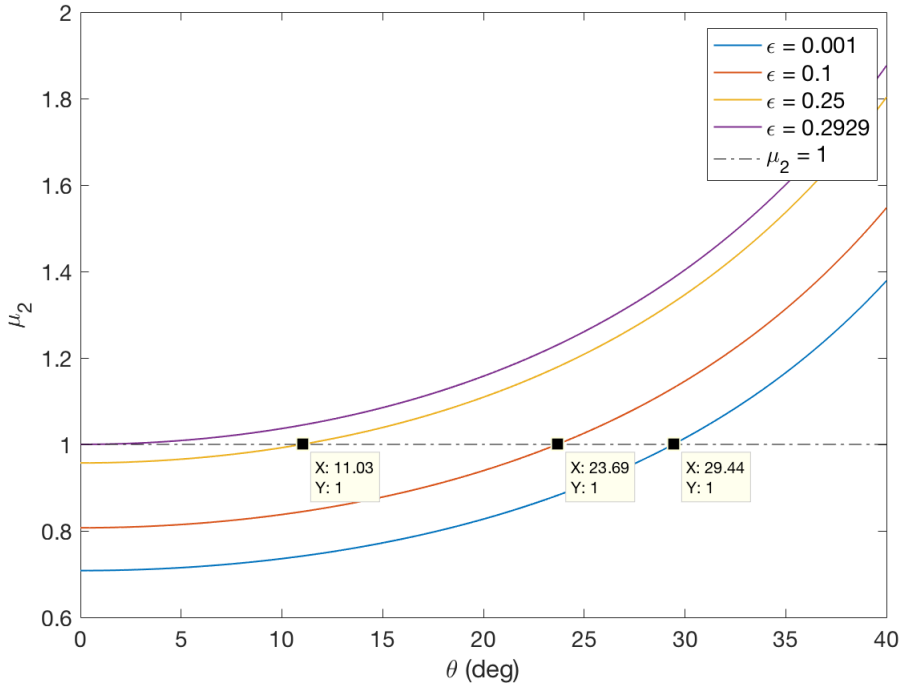

Figure 2.4: Mass reduction for a unit D-Bar [1]

2.3 Iterative Design of Robot Arm

Now that it has been established that both T-Bars and D-Bars have lower masses than a column bearing the same compressive load the next step is to utilize these as

building blocks to design the robot arm. The iterations are shown in Fig. 2.5(a).

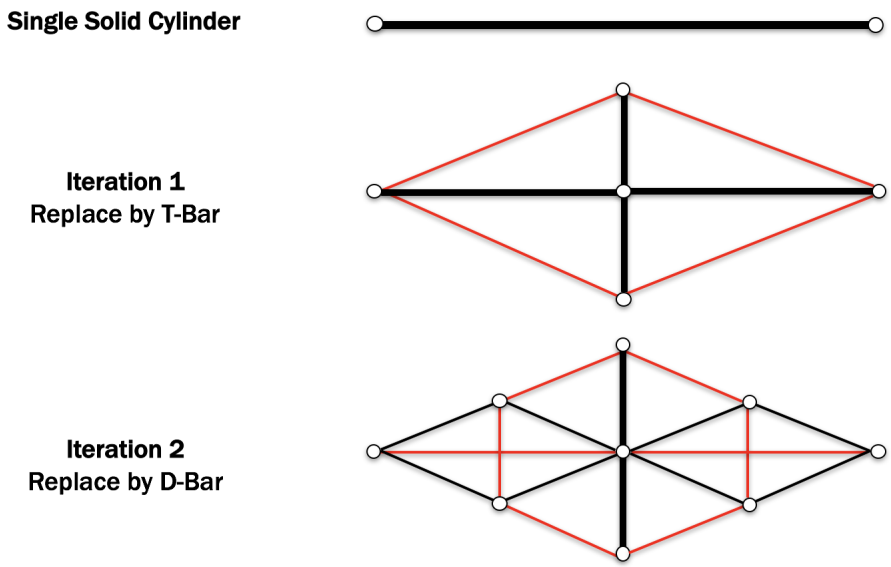

(a) Iterative design

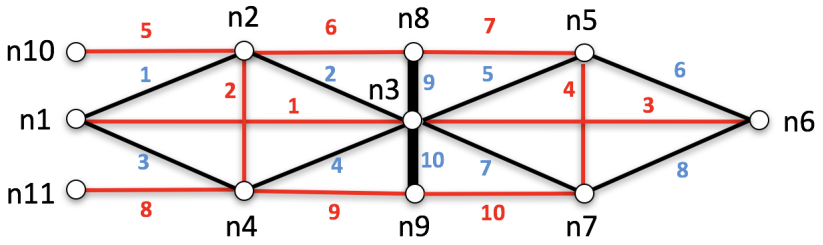

(b) Final design

Figure 2.5: Design of robot arm

In the first step a single column is replaced by a single T-Bar, which is a minimal mass solution. In the second step, the horizontal bars of the T-Bar are replaced by D-Bars. This assembly now satisfies both mass minimization and extensibility and retractability requirements. The process could go on further but for the sake of simplicity the iteration is terminated in this step. Additional strings (5 and 8)

provide further stability and controllability to the structure.

The final design is shown in Fig. 2.5(b). In this design there are 10 bars, 10 strings and 11 nodes. The T-Bars and D-bars are of unequal lengths. The bars are numbered in blue and the strings are numbered in red. The nodes $\mathbf{n_1}, \mathbf{n_{10}}$ and $\mathbf{n_{11}}$ are pinned whereas other nodes are free to move in the x-y plane. The D-Bars are modified to remove the central node and replace the four strings with two strings. External forces and disturbances are applied on node $\mathbf{n_6}$. The bar and string connectivity matrices are given by

$$\mathbf{C_b} = \begin{bmatrix} -1 & 1 & 0 & 0 & 0 & 0 & 0 & 0 & 0 & 0 & 0 \\ 0 & -1 & 1 & 0 & 0 & 0 & 0 & 0 & 0 & 0 & 0 \\ -1 & 0 & 0 & 1 & 0 & 0 & 0 & 0 & 0 & 0 & 0 \\ 0 & 0 & 1 & -1 & 0 & 0 & 0 & 0 & 0 & 0 & 0 \\ 0 & 0 & -1 & 0 & 1 & 0 & 0 & 0 & 0 & 0 & 0 \\ 0 & 0 & 0 & 0 & -1 & 1 & 0 & 0 & 0 & 0 & 0 \\ 0 & 0 & -1 & 0 & 0 & 0 & 1 & 0 & 0 & 0 & 0 \\ 0 & 0 & 0 & 0 & 0 & 1 & -1 & 0 & 0 & 0 & 0 \\ 0 & 0 & -1 & 0 & 0 & 0 & 0 & 1 & 0 & 0 & 0 \\ 0 & 0 & -1 & 0 & 0 & 0 & 0 & 0 & 1 & 0 & 0 \end{bmatrix} \tag{2.27}$$

$$\mathbf{C_s} = \begin{bmatrix} -1 & 0 & 1 & 0 & 0 & 0 & 0 & 0 & 0 & 0 & 0 \\ 0 & -1 & 0 & 1 & 0 & 0 & 0 & 0 & 0 & 0 & 0 \\ 0 & 0 & -1 & 0 & 0 & 1 & 0 & 0 & 0 & 0 & 0 \\ 0 & 0 & 0 & 0 & -1 & 0 & 1 & 0 & 0 & 0 & 0 \\ 0 & 1 & 0 & 0 & 0 & 0 & 0 & 0 & 0 & -1 & 0 \\ 0 & -1 & 0 & 0 & 0 & 0 & 0 & 1 & 0 & 0 & 0 \\ 0 & 0 & 0 & 0 & 1 & 0 & 0 & -1 & 0 & 0 & 0 \\ 0 & 0 & 0 & 1 & 0 & 0 & 0 & 0 & 0 & 0 & -1 \\ 0 & 0 & 0 & -1 & 0 & 0 & 0 & 0 & 1 & 0 & 0 \\ 0 & 0 & 0 & 0 & 0 & 0 & 1 & 0 & -1 & 0 & 0 \end{bmatrix} \tag{2.28}$$

Material is selected based on buckling and minimal mass constraints presented in the previous sections. Bars are made out of Al-2014 alloy and strings out of Stainless Steel. The following table illustrates some of the selected specifications.

Property	**Bar**	**String**
Geometry	Solid cylindrical rod	Cylindrical wire
Length (m)	0.25 (Bars 1-8) 0.125 (Bars 9-10)	(variable control parameter)
Radius (m)	0.005	0.001
Material	Al-2014 alloy	Stainless steel
Density (kg/m^3)	2800	7800
Modulus of Elasticity (GPa)	70	200
Yield Strength (MPa)	240	215

Table 2.1: Geometry and material properties

2.4 Minimal Mass Analysis

This section presents a comparison of the minimal masses of the robot design with a solid cylindrical column subject to compressive load. Although the robot is designed for minimal mass in compression, the transverse load case is also presented here.

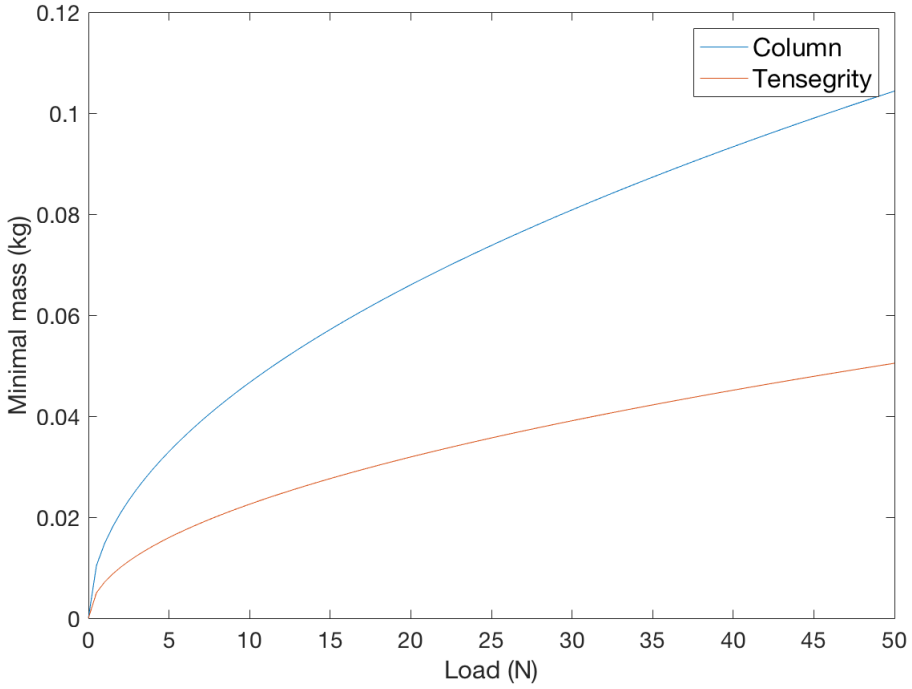

Figure 2.6: Minimal mass with varying compressive load

2.4.1 Compressive Load

A compressive load acts in the $-x$ direction on node $\mathbf{n_6}$. The equilibrium equation (1.4) gives the force densities in the members from which the bar forces can be calculated. These bar forces are fed into (2.1) to obtain the minimal mass of the

bars. Fig. 2.6 shows the comparison between the minimal masses of the tensegrity structure and an equivalent column bearing the same load. It was observed that the minimal mass for the tensegrity robot arm is substantially less than the column.

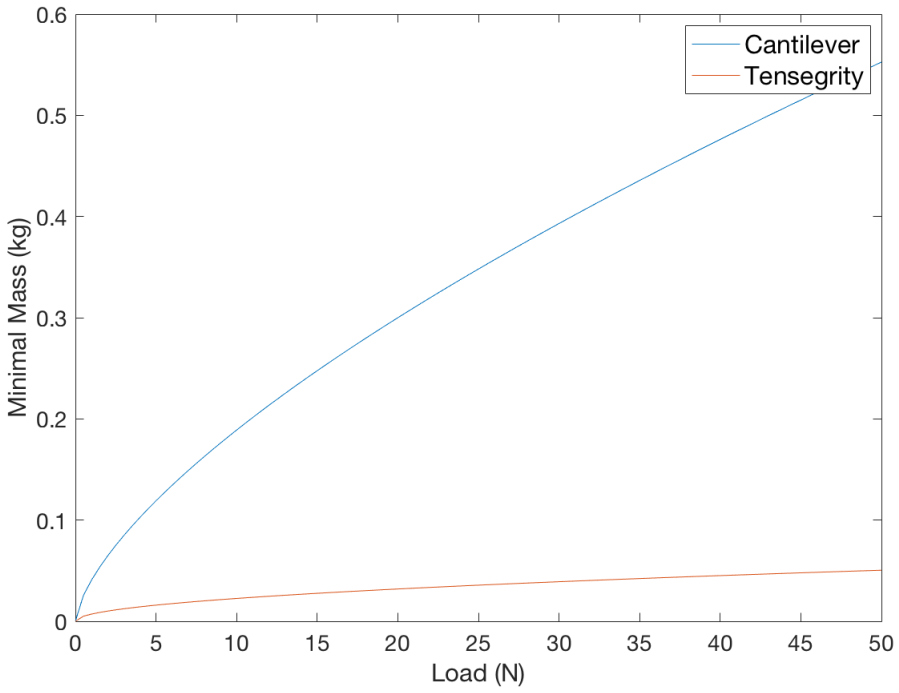

Figure 2.7: Minimal mass with varying transverse load

2.4.2 Transverse Load

In case of a transverse load the external load will be applied at node $\mathbf{n_6}$ in the $-y$ direction. The minimal mass case will be compared to a cantilever beam subject to the same bending load. From the flexure formula $\frac{\sigma_y}{y} = \frac{M_b}{I}$ the minimal mass of a

cantilever beam can be expressed as

$$m_c = \left(\frac{16\pi\rho^3 l_0^3 M_b^2}{\sigma_y^2} \right)^{\frac{1}{3}} \tag{2.29}$$

where $I = \frac{\pi r^4}{4}$ is the moment of inertia of the beam, σ_y is the allowable yield stress, y is the fiber distance and M_b is the maximum bending moment due to the applied load. The loads in the tensegrity robot arm are calculated similar to the compressive load case and compared against the cantilever beam in Fig. 2.7. It was observed that the tensegrity robot has lower minimal mass for all transverse loads. It must be noted that for cantilever beams, the minimal mass tensegrity design is a Mitchell truss [1].

[1] See [1] for design of cantilever beams.

3. DYNAMICS

In this work, minimal coordinates have been used to formulate the dynamics of the tensegrity robot. The minimal coordinates are a set of angles and angular velocities that completely describe the state of the system at any instant. Lagrange's equations of motion have been used to develop the dynamics.

3.1 Kinematics

3.1.1 Minimal coordinates

The minimal coordinates or the degrees of freedom of the robot arm are represented by the angles $\alpha_i, \theta_i, \phi_i$ where $i = 1, 2$ as shown in Fig 3.1. These set of coordinates can completely represent the position and orientation of the bars and strings with respect to an inertial reference frame n^+. There are $k = 6$ degrees of freedom in total. Here onwards, the generalized coordinates and velocities may be represented by

$$\mathbf{q} = [\alpha_1, \alpha_2, \theta_1, \theta_2, \phi_1, \phi_2]^T \tag{3.1}$$

$$\dot{\mathbf{q}} = [\dot{\alpha}_1, \dot{\alpha}_2, \dot{\theta}_1, \dot{\theta}_2, \dot{\phi}_1, \dot{\phi}_2]^T \tag{3.2}$$

3.1.2 Node Matrix

Fig 3.2 shows the numbering of the nodes, bars and strings. The bars are numbered in blue and the strings in red. The node matrix $\mathbf{N} \in \mathbb{R}^{3\times n}$ is expressed as follows, and elaborated in Appendix A.

$$\mathbf{N} = [\mathbf{n_1} \quad \mathbf{n_2} \quad ... \quad \mathbf{n}_\beta] \tag{3.3}$$

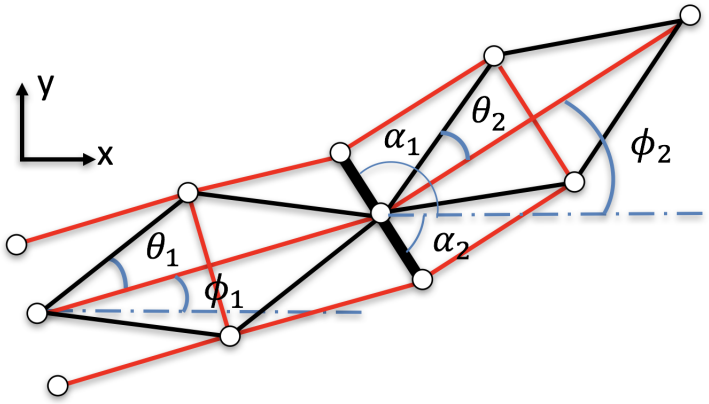

Figure 3.1: Minimal coordinates

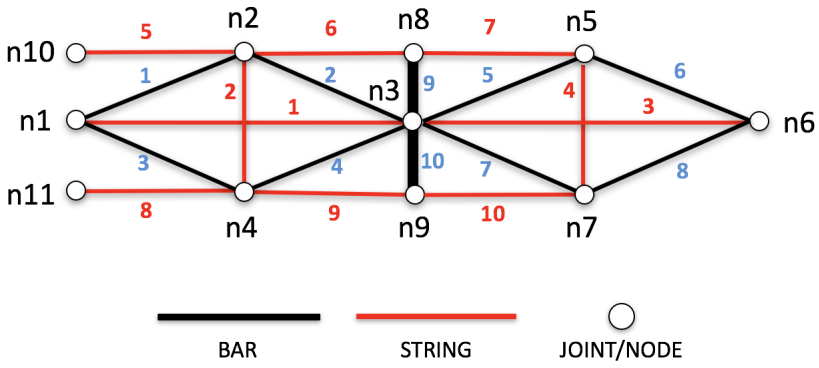

Figure 3.2: Tensegrity robot: Bars, Strings and Nodes

3.1.3 Connectivity Matrices

The bar and string connectivity matrices are represented as per Eq. (2.27-2.28).

3.1.4 Bar and String Matrices

The bar and string vectors can be represented in matrix format as follows

$$\mathbf{B} = \mathbf{N}\mathbf{C}_\mathbf{b}^\mathbf{T} \tag{3.4}$$

$$\mathbf{S} = \mathbf{N}\mathbf{C}_\mathbf{s}^\mathbf{T} \tag{3.5}$$

3.1.5 Bar Mass Centers

The position vector $\mathbf{r_i}$ from the origin to the mass center of the i_{th} bar can be expressed as

$$\mathbf{r_i} = \frac{\mathbf{n_j} + \mathbf{n_k}}{2}$$

where $\mathbf{n_j}, \mathbf{n_k}$ are the starting and ending nodes of the bar. In matrix form this is represented as $\mathbf{R} \in \mathbb{R}^{3\times\beta}$

$$\mathbf{R} = \mathbf{N}\mathbf{C}_\mathbf{r}^\mathbf{T} \tag{3.6}$$

where

$$\mathbf{C_r} = \frac{1}{2}|\mathbf{C_b}|$$

3.1.6 Node, Bar and Mass Center Velocities

The time derivatives of $\mathbf{N}, \mathbf{B}, \mathbf{R}$ are expressed as follows.

$$\dot{\mathbf{N}} = [\dot{\mathbf{n}}_\mathbf{1} \quad \dot{\mathbf{n}}_\mathbf{2} \quad ... \quad \dot{\mathbf{n}}_\beta] \tag{3.7}$$

where $\dot{\mathbf{n}}_\mathbf{i} = \frac{\mathbf{d}}{\mathbf{dt}}(\mathbf{n_i})$ is the translational velocity of the i^{th} node coordinatized in the inertial reference frame. Consequently,

$$\dot{\mathbf{B}} = \dot{\mathbf{N}}\mathbf{C}_\mathbf{b}^\mathbf{T} \tag{3.8}$$

$$\dot{\mathbf{S}} = \dot{\mathbf{N}}\mathbf{C}_\mathbf{s}^\mathbf{T} \tag{3.9}$$

$$\dot{\mathbf{R}} = \dot{\mathbf{N}}\mathbf{C}_\mathbf{r}^\mathbf{T} \tag{3.10}$$

3.2 Dynamics

Lagrange's equations of motion have been used to formulate the dynamics of the tensegrity robot arm with the following assumptions.

1. Each bar is assumed to be a rigid cylindrical solid rod. The mass of each bar is represented as m_i.

2. Each string is assumed to be massless and elastic, obeying Hooke's law of elasticity.

3. There is no rotation of the bars along their longitudinal axes.

4. The joints between bars are free from friction and damping.

The dynamics formulation is presented below.

3.2.1 Moment of Inertia

The moments of inertia are calculated with respect to the principal frame b^+ of the bars at their mass center. If the mass, radius and length of each bar be represented by m_i, $r_{b,i}$ and L_i then the moments of inertia about their principal axes

are given by

$$I_a = \frac{1}{2} m_i r_{b,i}^2$$
$$I_t = \frac{1}{12} m_i L_i^2$$

The moment of inertia tensor for a particular bar is given by

$$\mathbf{I} = \begin{bmatrix} I_a & 0 & 0 \\ 0 & I_t & 0 \\ 0 & 0 & I_t \end{bmatrix} \tag{3.11}$$

3.2.2 Angular Velocity

The angular velocities of the bars can be represented by the matrix $\mathbf{\Omega} \in \mathbb{R}^{3\times\beta}$ with the i^{th} column representing the angular velocity of the i^{th} bar.

$$\mathbf{\Omega} = [\omega_{\mathbf{1}} \quad \omega_{\mathbf{2}} \quad ... \quad \omega_\beta] \tag{3.12}$$

The expressions for $\omega_{\mathbf{1}}, \omega_{\mathbf{2}} ... \omega_\beta$ are given in Appendix A.

3.2.3 Angular Momentum

The angular momentum of the i^{th} bar with angular velocity ω_i is given by

$$\mathbf{h_i} = \mathbf{I}\omega_\mathbf{i}$$

Collectively, the angular momenta of the bars can be written in matrix format $\mathbf{H} \in \mathbb{R}^{3\times\beta}$ where each column represents the angular momentum of the i^{th} bar.

$$\mathbf{H} = \mathbf{I\Omega} \tag{3.13}$$

3.2.4 Kinetic Energy

The translational and rotational kinetic energies of each bar is expressed as

$$T_{i,trans} = \frac{1}{2} m_i ||\dot{\mathbf{r}}_i||^2 \qquad T_{i,rot} = \frac{1}{2}\omega_{\mathbf{i}} \cdot \mathbf{h_i}$$

where $\dot{\mathbf{r}}_\mathbf{i}$ is the i^{th} column of $\dot{\mathbf{R}}$. The total kinetic energy of the i^{th} bar is given by

$$T_i = \sum_{i=1}^{\beta} (T_{i,trans} + T_{i,rot})$$

In matrix form

$$\mathbf{T} = \frac{1}{2}\hat{\mathbf{m}} \cdot diag(\dot{\mathbf{R}}^\mathbf{T}\dot{\mathbf{R}}) + \frac{1}{2} diag(\mathbf{H}^\mathbf{T}\mathbf{\Omega}) \tag{3.14}$$

where $\mathbf{T} \in \mathbb{R}^{\beta\times 1}$ and

$$\hat{\mathbf{m}} = \begin{bmatrix} m_1 & & 0 \\ & \ddots & \\ 0 & & m_\beta \end{bmatrix}$$

It must be noted that $diag(\mathbf{X})$ is a matrix diagonalization operator that extracts the diagonal elements of the square matrix $\mathbf{X}$.

3.2.5 Potential Energy

In the presence of gravity the bars are subject to gravitational potential forces and must be catered to on the left hand side of Lagrange's equations. If gravity acts in the $-z$ direction then the gravitational potential energy of each bar with respect

to a datum is given by

$$V_i = m_i \mathbf{p_i} \cdot \mathbf{g}$$

where $\mathbf{p_i} = \mathbf{r_i} + [0, p, 0]^T$ is the position vector of the bar mass center from the inertial frame and $\mathbf{g}$ is the acceleration due to gravity. In matrix form,

$$\mathbf{V} = \hat{\mathbf{m}}\mathbf{P^T}\mathbf{g} \tag{3.15}$$

where $\mathbf{V} \in \mathbb{R}^{\beta \times 1}$ and $\mathbf{P} \in \mathbb{R}^{3 \times \beta}$ is a matrix which contains $\mathbf{p_i}$ in its columns.

3.2.6 Lagrangian Function

The Lagrangian function is expressed as the difference between the sum of kinetic energies and the sum of gravitational potential energies of the bars.

$$L = \sum_{i=1}^{\beta} \mathbf{T} - \mathbf{V} \tag{3.16}$$

$$= \sum_{i=1}^{\beta} \frac{1}{2}\hat{\mathbf{m}} \cdot diag(\dot{\mathbf{R}}^{\mathbf{T}}\dot{\mathbf{R}}) + \frac{1}{2} diag(\mathbf{H^T\Omega}) - \hat{\mathbf{m}}\mathbf{D^T}\mathbf{g} \tag{3.17}$$

3.2.7 String Forces

The strings are assumed to obey Hooke's law of elasticity and are also associated with damping. If $\mathbf{s_i}$ be the vector representing the i^{th} string then the string force is given by

$$\mathbf{f_{s,i}} = \begin{cases} k_i(||\mathbf{s_i}|| - u_i)\hat{\mathbf{s}}_\mathbf{i} + c_i\dot{\mathbf{s}}_\mathbf{i} & \text{if } ||\mathbf{s_i}|| > u_i \\ \mathbf{0} & \text{otherwise} \end{cases} \tag{3.18}$$

where k_i and c_i are the string stiffness and damping constants, $\hat{\mathbf{s}}_\mathbf{i}$ is the unit

vector in the direction of $\mathbf{s_i}$ and u_i is the rest length of the i^{th} string.

3.2.8 Forces at the Nodes

External forces may be applied on the system. In that case the net force acting on each node is the summation of the string forces, the external forces and disturbances acting at that node. If $\mathbf{w_i}, \mathbf{d_i}$ be the external forces and disturbances acting on the i^{th} node then the net force is given by

$$\mathbf{F_i} = \sum \mathbf{f_{s,i}} + \mathbf{w_i} + \mathbf{d_i} \tag{3.19}$$

3.2.9 Generalized Forces

The work rate expression is obtained by the dot product of the forces at nodes and the position vectors of the nodes. The generalized forces Q_k are the coefficients of the generalized velocities in the work rate expression.

$$\dot{W} = \sum_{i=1}^{n} \mathbf{F_i} \cdot \mathbf{n_i} \tag{3.20}$$

$$Q_k = \frac{\partial \dot{W}}{\partial \mathbf{q_k}} \tag{3.21}$$

3.2.10 Equations of Motion

Lagrange's equations of motion are given by

$$\frac{d}{dt}\left(\frac{\partial L}{\partial \dot{\mathbf{q}}_\mathbf{k}}\right) - \frac{\partial L}{\partial \mathbf{q_k}} = Q_k \tag{3.22}$$

There will be k equations of motion containing time derivatives of $\mathbf{q}$ and $\dot{\mathbf{q}}$. These equations can be reduced to a mass matrix form as follows:

$$\mathbf{M}(\mathbf{q})\ddot{\mathbf{q}} = \mathbf{f}(\mathbf{q}, \dot{\mathbf{q}}, \mathbf{u}) \tag{3.23}$$

where $\mathbf{M}(\mathbf{q})$ is the mass matrix which depends on the generalized coordinates and $\mathbf{f}(\mathbf{q}, \dot{\mathbf{q}}, \mathbf{u})$ represents the right side of the equation. While solving the dynamics through an integration algorithm such as *Runge-Kutta*, both $\mathbf{M}$ and $\mathbf{f}$ can be numerically computed at each timestep to obtain the second derivatives of $\mathbf{q}$.

3.3 Simulation

Examples of dynamics simulation are presented to demonstrate the evolution of state variables, string fores and visualize the behavior of the structure over time. The simulations were performed using MATLAB's ode45 algorithm for different external loads.

3.3.1 Compressive Load

The first example is simulation with a compressive load acting at node $\mathbf{n_6}$. There are 11 nodes in the structure and the node matrix was defined as per (3.7). Based on the geometry of the structure, the dynamics was formulated as discussed in the previous section.

An external compressive load of $200N$ was applied in the $-x$ direction. Gravity was assumed to act in the $-z$ direction. The simulation was performed for $1s$ and the results are presented in Fig. 3.4-3.5. The initial states were $\mathbf{q_0} = [90°, -90°, 40°, 40°, 0°, 0°]^T$ and $\dot{\mathbf{q}}_\mathbf{0} = [0, 0, 0, 0, 0, 0]^T$ as shown in Fig. 3.3. The parameters used to define the strings are listed in Table 3.1.

It was observed in Fig. 3.4 that the states and their derivatives stabilize over

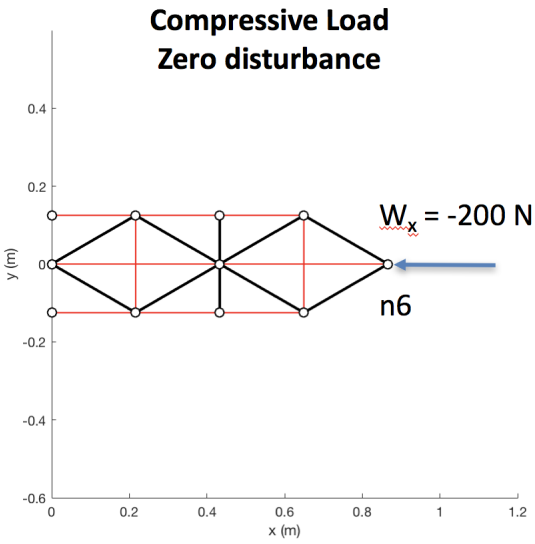

Figure 3.3: Compressive load acting at node n_6

String No.	**k** (kN/m)	**c** (N/m/s)	**u** (m)
1	9	30	0.433
2	16	30	0.2425
3	9	30	0.4330
4	16	30	0.2475
5	18	30	0.2011
6	18	30	0.2088
7	18	30	0.2088
8	18	30	0.2165
9	18	30	0.2165
10	18	30	0.2165

Table 3.1: String properties

time signifying that the chosen values of k and c are sufficient to reach a stable equilibrium. The α_i states were stabilized by strings 6, 7 ,8 and 9 which explains the spikes in the forces in these strings (Fig. 3.5). The θ_i states were stabilized by strings 2 and 4 which participated in bearing most of the external load. All other

strings had zero loads, i.e. were slack. In addition, the string forces for these strings did not start at zero due to the presence of prestress. The ϕ_i states did not change as the structure did not undergo geometrical buckling.

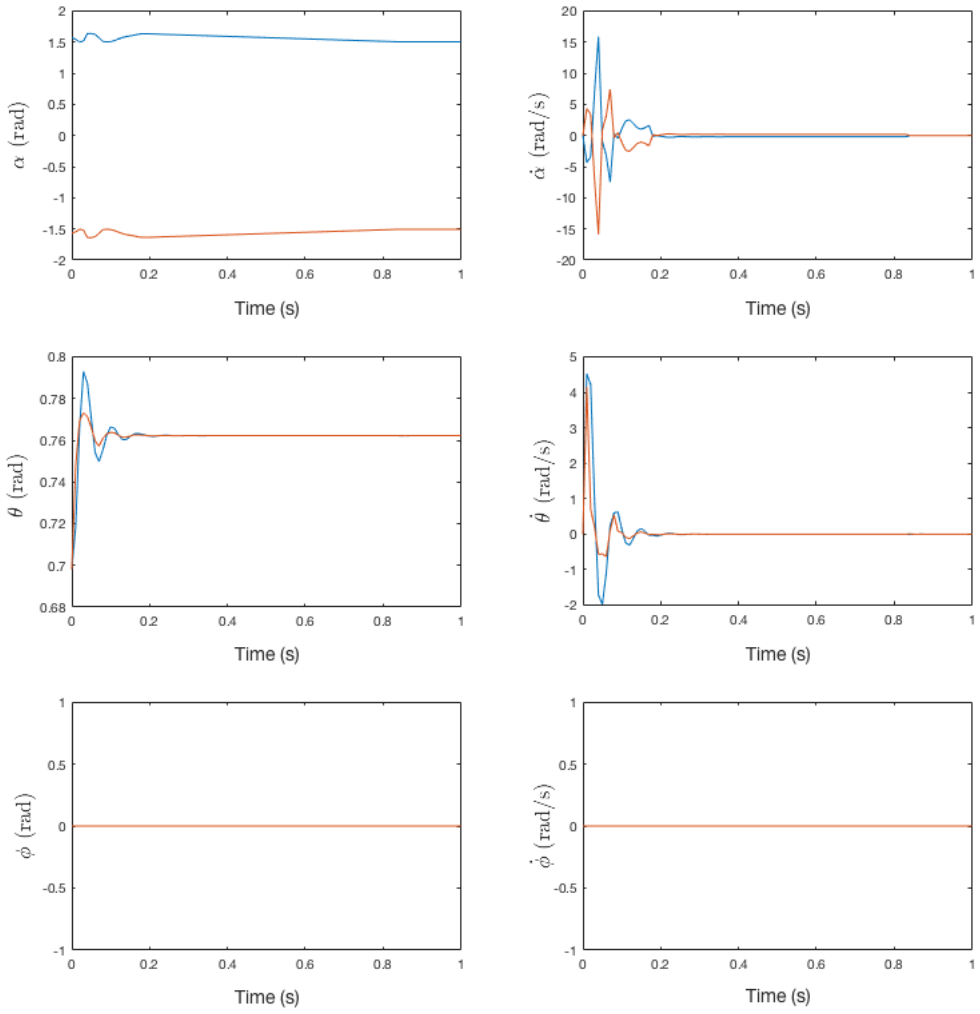

Figure 3.4: Evolution of states: Compressive Load

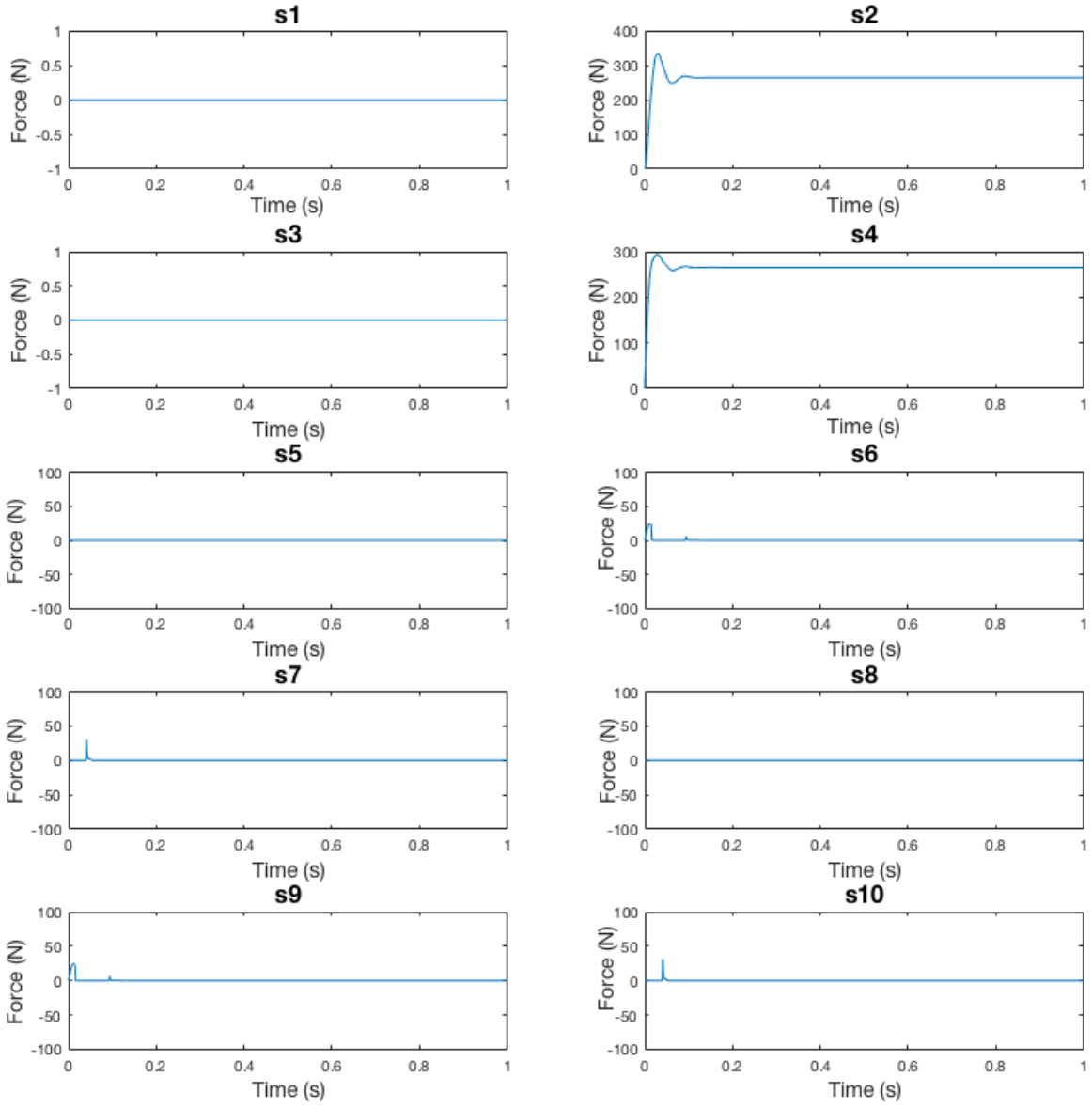

Figure 3.5: String forces: Compressive Load

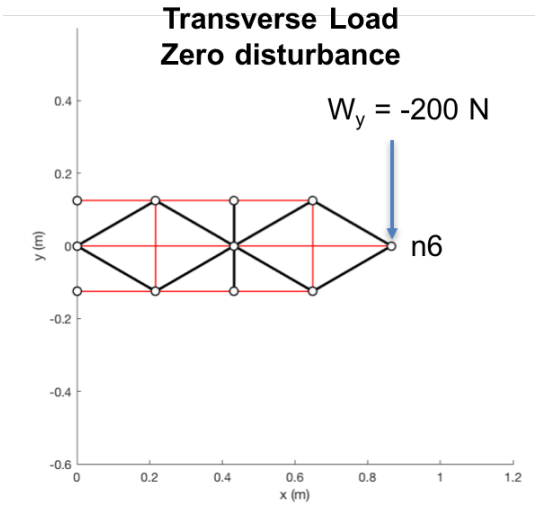

Figure 3.6: Transverse load acting at node n_6

3.3.2 Transverse Load

A transverse load of $200N$ was applied in the $-y$ direction to observe the behavior of the structure. Fig. 3.6 shows the initial state at $t = 0s$. The initial state values were $\mathbf{q_0} = [90°, -90°, 30°, 30°, 0°, 0°]^T$ and $\dot{\mathbf{q}}_\mathbf{0} = [0, 0, 0, 0, 0, 0]^T$. After simulating for $1s$ the structure was able to achieve a stable equilibrium with the unpinned nodes moving in the $-y$ direction The states evolved as per Fig. 3.7. The string forces presented in Fig. 3.8 showed that the strings 2, 4, 5, 6, 7 were loaded at equilibrium while the rest were unloaded. This complied with the string forces obtained after solving the equilibrium equation (1.4).

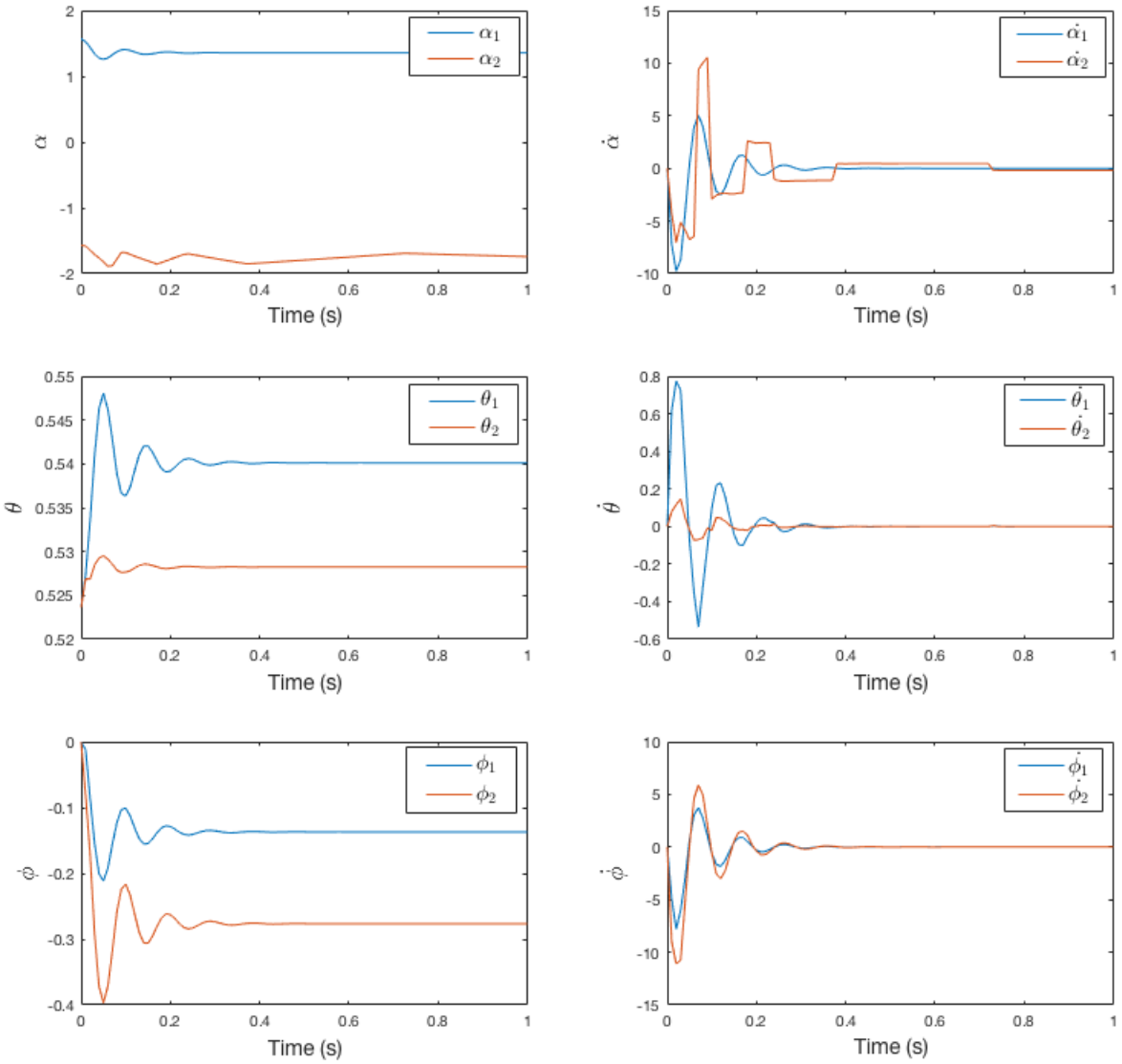

Figure 3.7: Evolution of states: Transverse Load

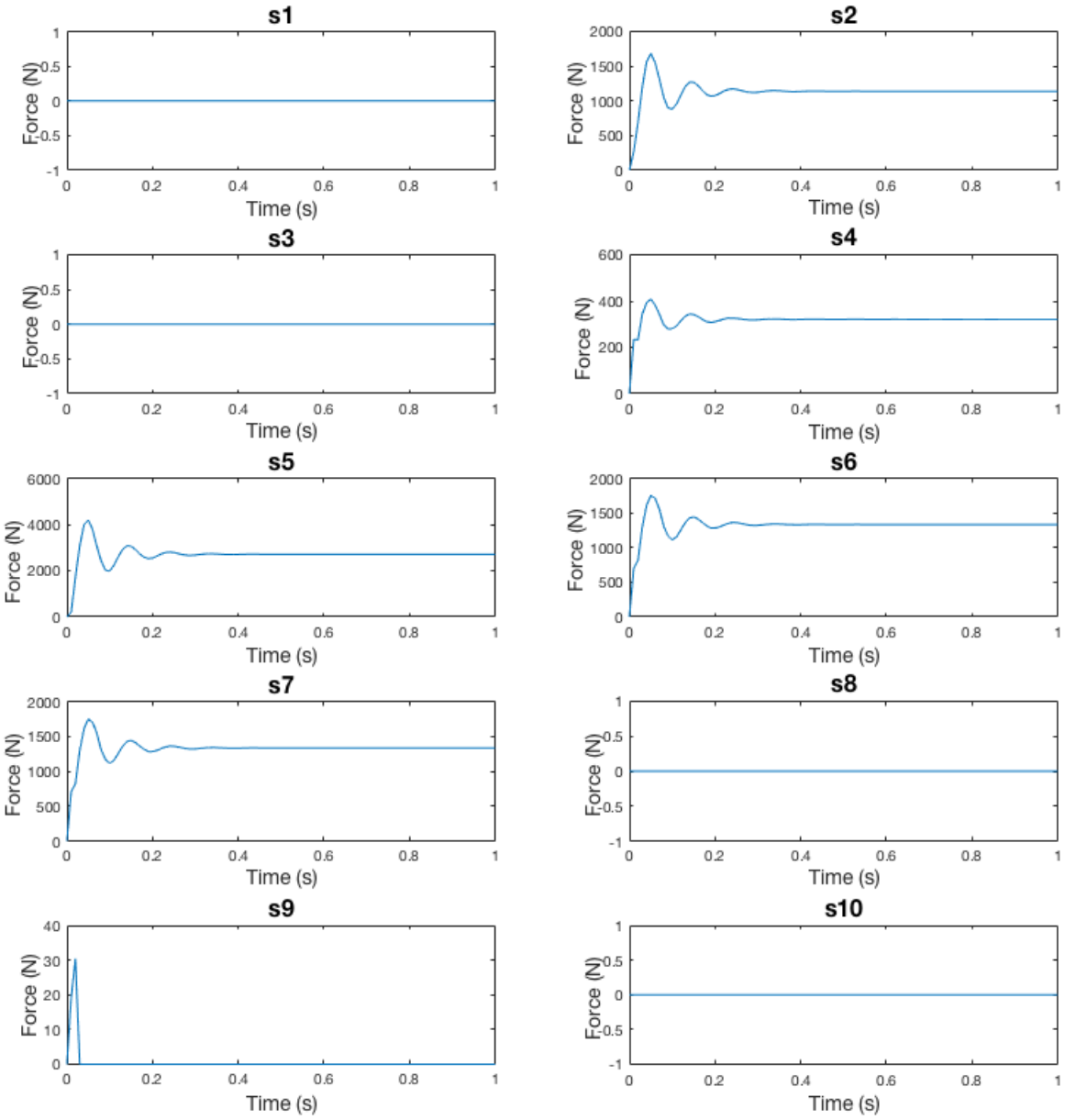

Figure 3.8: String forces: Transverse Load

4. CONTROLS

The goal of this research work is to address the following controls problems:

1. Stabilization of the robot in the presence of disturbance and sensor noise.

2. Signal tracking with disturbance and noise.

The robot should be able to perform the above tasks while carrying a payload of specified mass. It may be assumed that the node $\mathbf{n_6}$ will house a gripper that will carry the payload. Gripper weight along with payload weight will act as an external load at $\mathbf{n_6}$. In addition this node may be subject to force disturbances, which in practical sense amounts to the gripper carrying a vibrating payload, or being subject to a wind disturbance. Note that disturbances are incorporated in the dynamics as per Eq. (3.19).

4.1 Definitions

Before setting up the control problem it is important to define and classify few parameters.

4.1.1 Plant

The Plant may refer to the dynamics of the tensegrity robot arm represented by ($k = 6$) second order nonlinear equations (Eq. 3.23) or $2k$ first order nonlinear equations , where k is the number of minimal coordinates. This nonlinear plant is the closest approximation to the actual robot.

4.1.2 States

These variables describe the mathematical states of the system. For this problem the states are the angular positions and velocities $\alpha_i, \theta_i, \phi_i, \dot{\alpha}_i, \dot{\theta}_i, \dot{\phi}_i$ as defined in Eq.

(3.1-3.2). The states will henceforth be represented by $\mathbf{x} \in \mathbb{R}^{2k\times 1}$.

$$\mathbf{x} = [\mathbf{q}, \dot{\mathbf{q}}]^T \tag{4.1}$$

4.1.3 Control Variables

The control variables are the string rest lengths that will be physically controlled by actuators. The control variables appear on the right side of the dynamics equation (3.23) and are represented by $\mathbf{u} \in \mathbb{R}^{\eta\times 1}$.

4.1.4 Outputs

Typically outputs will be a set of sensor generated signals $\mathbf{y} \in \mathbb{R}^{2n\times 1}$. These sensors may be gyroscopes and accelerometers that sense the position and orientation of the bars, or strain gauges that sense the forces in the strings.

4.1.5 Disturbances

Often the payload acting at node $\mathbf{n_6}$ would be subject to disturbances. The disturbance $\mathbf{d} \in \mathbb{R}^{2\times 1}$ in this design are the force disturbances acting at node $\mathbf{n_6}$ in the x and y directions.

4.1.6 Noise

The measured outputs will be subject to sensor noise represented by $\mathbf{n} \in \mathbb{R}^{2n\times 1}$ in this design.

The tensegrity dynamics is nonlinear in the state and control variables and needs to be linearized about an operating point (also called trim point) in order to apply linear control theory. The linearization process is described below.

4.2 Linearization

Linearization about an operating point is obtained using the analytical Jacobian method. A multi-variable function $g(a, b)$ can be expanded in Taylor series about an operating point $\bar{a}, \bar{b}$ with each term containing the successive derivatives of the independent variables. In the vicinity of the operating point the nonlinear terms can be approximated to be zero which makes the equation linear in the variables a and b.

$$g(a,b) = g(\bar{a},\bar{b}) + \left.\frac{\partial g}{\partial a}\right|_{\bar{a},\bar{b}} \delta a + \left.\frac{\partial g}{\partial b}\right|_{\bar{a},\bar{b}} \delta b + \dots$$

where δa and δb are the perturbations in a and b about the operating point. In case of the tensegrity system it is useful to segregate the disturbance terms from the control inputs in the right side of the dynamics equations (3.23). This segregation is essential to design the state space matrix. Hence, the right side of the dynamics equations will be represented by $\mathbf{f}(\mathbf{q}, \dot{\mathbf{q}}, \mathbf{d}, \mathbf{u})$ with $\mathbf{d}$ representing the disturbances. Now, if the operating point is defined as $\bar{\mathbf{p}} = \left[\bar{\mathbf{q}}, \bar{\dot{\mathbf{q}}}, \bar{\mathbf{d}}, \bar{\mathbf{u}}\right]$ then the functions $\mathbf{M}(\mathbf{q})$ and $\mathbf{f}(\mathbf{q}, \dot{\mathbf{q}}, \mathbf{d}, \mathbf{u})$ are linearized as follows

$$\mathbf{M}(\mathbf{q}) = \bar{\mathbf{M}} + \delta\mathbf{M} \tag{4.2}$$

$$\mathbf{f}(\mathbf{q}, \dot{\mathbf{q}}, \mathbf{d}, \mathbf{u}) = \bar{\mathbf{f}} + \delta\mathbf{f} \tag{4.3}$$

where

$$\bar{\mathbf{M}} = \mathbf{M}(\bar{\mathbf{q}}), \quad \bar{\mathbf{f}} = \mathbf{f}(\bar{\mathbf{q}}, \bar{\dot{\mathbf{q}}}, \bar{\mathbf{d}}, \bar{\mathbf{u}})$$

$$\delta\mathbf{M} = \sum_{i=1}^{2k} \left.\frac{\partial \mathbf{M}}{\partial \mathbf{q_i}}\right|_{\bar{\mathbf{q}}} \delta\mathbf{q_i}$$

$$\delta\mathbf{f} = \left.\frac{\partial \mathbf{f}}{\partial \mathbf{q}}\right|_{\bar{\mathbf{p}}} \delta\mathbf{q} + \left.\frac{\partial \mathbf{f}}{\partial \dot{\mathbf{q}}}\right|_{\bar{\mathbf{p}}} \delta\dot{\mathbf{q}} + \left.\frac{\partial \mathbf{f}}{\partial \mathbf{d}}\right|_{\bar{\mathbf{p}}} \delta\mathbf{d} + \left.\frac{\partial \mathbf{f}}{\partial \mathbf{u}}\right|_{\bar{\mathbf{p}}} \delta\mathbf{u}$$

The dynamics about the operating point can be written as

$$\ddot{\mathbf{q}} = \left(\bar{\mathbf{M}} + \delta\mathbf{M}\right)^{-1}\left(\bar{\mathbf{f}} + \delta\mathbf{f}\right) \tag{4.4}$$

With greater number of bars and strings, symbolic inversion of the mass matrix $\bar{\mathbf{M}} + \delta\mathbf{M}$ becomes computationally intensive. To avoid this penalty, the mass matrix can be numerically inverted at the operating point [8]. Consider the Woodbury matrix identity,

$$(A + UCV)^{-1} = A^{-1} - A^{-1}U(C^{-1} + VA^{-1}U)^{-1}VA^{-1} \tag{4.5}$$

Substituting A by $\bar{\mathbf{M}}$, V by $\delta\mathbf{M}$ and U, C with identity matrices the following expression is obtained

$$\left(\bar{\mathbf{M}} + \delta\mathbf{M}\right)^{-1} = \bar{\mathbf{M}}^{-1} - \bar{\mathbf{M}}^{-1}\delta\mathbf{M}\bar{\mathbf{M}}^{-1} \tag{4.6}$$

which does not involve symbolic inversion of matrices and is computationally faster. The dynamics can be written after combining Eq. (4.4) and (4.6) and ignoring the higher order terms that result after the expansion.

$$\ddot{\mathbf{q}} = \bar{\mathbf{M}}^{-1}\bar{\mathbf{f}} + \bar{\mathbf{M}}^{-1}\delta\mathbf{f} - \bar{\mathbf{M}}^{-1}\delta\mathbf{M}\bar{\mathbf{M}}^{-1}\bar{\mathbf{f}} \tag{4.7}$$

$$\delta\ddot{\mathbf{q}} = \bar{\mathbf{M}}^{-1}\delta\mathbf{f} - \bar{\mathbf{M}}^{-1}\delta\mathbf{M}\bar{\mathbf{M}}^{-1}\bar{\mathbf{f}} \tag{4.8}$$

Eq. (4.8) represents k second order linear equations which can be converted to $2k$ first order linear ODEs as below

$$\delta\dot{\mathbf{x}} = \mathbf{A}\delta\mathbf{x} + \mathbf{B_d}\delta\mathbf{d} + \mathbf{B_u}\delta\mathbf{u} \tag{4.9}$$

where

$$\delta\mathbf{x} = \begin{bmatrix} \delta\mathbf{q} \\ \delta\dot{\mathbf{q}} \end{bmatrix} \quad \mathbf{A} = \begin{bmatrix} \mathbf{0} & \mathbf{I} \\ \frac{\partial}{\partial\mathbf{x}}\left(\delta\ddot{\mathbf{q}}\right) & \end{bmatrix}$$

$$\mathbf{B_d} = \begin{bmatrix} \mathbf{0} \\ \frac{\partial}{\partial\mathbf{d}}\left(\delta\ddot{\mathbf{q}}\right) \end{bmatrix} \quad \mathbf{B_u} = \begin{bmatrix} \mathbf{0} \\ \frac{\partial}{\partial\mathbf{u}}\left(\delta\ddot{\mathbf{q}}\right) \end{bmatrix}$$

The outputs of the system are the signals from the sensors that measure nodal position and velocity. The nonlinear outputs are given by $\mathbf{y}$ [1]

$$\mathbf{y} = \begin{bmatrix} \text{vec}(\mathbf{N}) \\ \text{vec}(\dot{\mathbf{N}}) \end{bmatrix} \tag{4.10}$$

where the vec($\mathbf{X}$) operator rearranges the elements of the matrix $\mathbf{X}$ in vector format. The linearized output equations are therefore

$$\delta\mathbf{y} = \mathbf{C}\delta\mathbf{x} + \mathbf{D_d}\delta\mathbf{d} + \mathbf{D_u}\delta\mathbf{u} \tag{4.11}$$

where

$$\mathbf{C} = \left.\frac{\partial\mathbf{y}}{\partial\mathbf{x}}\right|_{\bar{\mathbf{p}}} \quad \mathbf{D_d} = \mathbf{0} \quad \mathbf{D_u} = \mathbf{0}$$

Eqs. (4.9) and (4.11) represent the state-space equations of the system.

4.3 Stabilization

The stabilization problem involved stabilization of nodes of the structure about the following operating point in the presence of disturbance and sensor noise. The

[1] Only x and y components of $\mathbf{N}$ and $\dot{\mathbf{N}}$ were considered

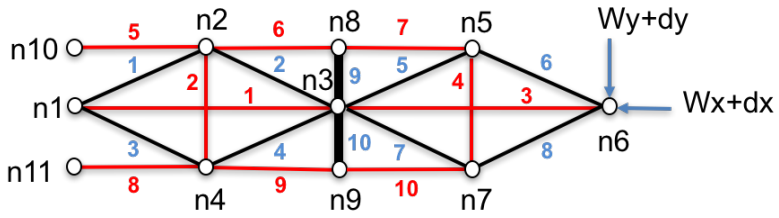

Figure 4.1: Stabilization with disturbance and noise

trim values for control were obtained using Eq. (1.4).

$$\bar{\mathbf{q}} = [90, -90, 18.2, 18.2, 0, 0]^T \text{ deg}$$

$$\bar{\dot{\mathbf{q}}} = [0, 0, 0, 0, 0, 0]^T \text{ deg/s}$$

$$\bar{\mathbf{d}} = [0, 0]^T \text{ N}$$

$$\bar{\mathbf{u}} = [0.4750, 0.0647, 0.4489, 0.1061, 0.0484, 0.1453, 0.1453, 0.2421, 0.2421, 0.2421]^T \text{ m}$$

4.3.1 H2 Optimal Control

While choosing a controller it was necessary to focus on performance goals. Since it was necessary to achieve performance with minimum energy spent in the actuators optimal control theory was a suitable choice. H2 control theory [9] focuses on designing a controller that rejects an extraneous signal $\mathbf{w}$ while minimizing the 2-norm of the signal $\mathbf{z}$. The extraneous signals comprised of force disturbances $\mathbf{d}$ at the nodes and measurement noise $\mathbf{n}$ in the sensors. The noise did not cause direct feed-through to the signal $\mathbf{z}$, instead got added with the output signal $\mathbf{y}$ to generate $\mathbf{y_m}$ which was the measured outputs from the sensors.

Fig. 4.2 shows the block diagram for the H2 control system. The extraneous signal $\mathbf{w}$ and control input $\mathbf{u}$ were inputs to the plant $\mathbf{G}$. The signals to minimize were the position of the nodes $\mathbf{N}$ and the control signals $\mathbf{u}$. The outputs of the plant

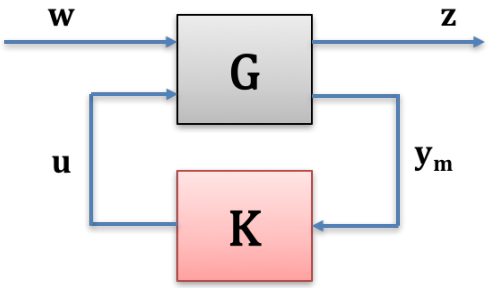

Figure 4.2: Block diagram for H2 control system

were the signal $\mathbf{z}$ and the measured outputs $\mathbf{y_m}$. The relationships are summarized below

$$\mathbf{w} = [\mathbf{d}, \mathbf{n}]^T$$

$$\mathbf{z} = [\mathbf{N}, \mathbf{u}]^T$$

$$\mathbf{y_m} = \mathbf{y} + \mathbf{n}$$

The plant dynamics were given by

$$\delta\dot{\mathbf{x}} = \mathbf{A}\delta\mathbf{x} + \mathbf{B_w}\delta\mathbf{w} + \mathbf{B_u}\delta\mathbf{u} \tag{4.12}$$

$$\delta\mathbf{z} = \mathbf{C_z}\delta\mathbf{x} + \mathbf{D_{wz}}\delta\mathbf{w} + \mathbf{D_{uz}}\delta\mathbf{u} \tag{4.13}$$

$$\delta\mathbf{y} = \mathbf{C_y}\delta\mathbf{x} + \mathbf{D_{wy}}\delta\mathbf{w} + \mathbf{D_{uy}}\delta\mathbf{u} \tag{4.14}$$

where $\mathbf{D_{wz}} = \mathbf{D_{uy}} = \mathbf{0}$ (no direct feed-through terms). It must be noted that

$$\mathbf{y} = \bar{\mathbf{y}} + \delta\mathbf{y}$$

$$\mathbf{u} = \bar{\mathbf{u}} + \delta\mathbf{u}$$

where $\bar{\mathbf{y}}, \bar{\mathbf{u}}$ are the values at the operating point. The controller dynamics was

$$\delta\dot{\mathbf{x}}_\mathbf{c} = \mathbf{A_c}\delta\mathbf{x_c} + \mathbf{B_c}\mathbf{y_m} \tag{4.15}$$

$$\delta\mathbf{u} = \mathbf{C_c}\delta\mathbf{x_c} \tag{4.16}$$

The above relationships led to the following state-space matrix representation of the H2 plant and controller.

$$\mathbf{G} = \left[\begin{array}{c|cc} \mathbf{A} & \mathbf{B_w} & \mathbf{B_u} \\ \hline \mathbf{C_z} & \mathbf{0} & \mathbf{D_{uz}} \\ \mathbf{C_y} & \mathbf{D_{wy}} & \mathbf{0} \end{array}\right] \tag{4.17}$$

$$\mathbf{K} = \left[\begin{array}{c|c} \mathbf{A_c} & \mathbf{B_c} \\ \hline \mathbf{C_c} & \mathbf{0} \end{array}\right] \tag{4.18}$$

The construction of optimal controller $\mathbf{K}$ resulted from the steps mentioned in [7], by minimizing the 2-norm of the transfer function $\mathbf{G_{w\to z}}$

$$||\mathbf{G_{w\to z}}||_2 = \left(\frac{1}{2\pi}\int_{-\infty}^{\infty} \mathbf{trace}\left[\mathbf{G}(j\omega)^*\mathbf{G}(j\omega)\right] d\omega\right)^{1/2}$$

subject to weights of the components of the signal $\mathbf{z}$, which in this case, were unity. Defining the Hamiltonian matrices $\mathbf{H_2}$ and $\mathbf{J_2}$ by

$$\mathbf{H_2} = \begin{bmatrix} \mathbf{A} & -\mathbf{B_u}\mathbf{B_u^T} \\ -\mathbf{C_z}\mathbf{C_z^T} & -\mathbf{A^T} \end{bmatrix} \qquad \mathbf{J_2} = \begin{bmatrix} \mathbf{A^T} & -\mathbf{C_y^T}\mathbf{C_y} \\ -\mathbf{B_w}\mathbf{B_w^T} & -\mathbf{A} \end{bmatrix}$$

and the Riccatti solutions $\mathbf{X_2} = \mathbf{Ric}(\mathbf{H_2})$, $\mathbf{Y_2} = \mathbf{Ric}(\mathbf{J_2})$. Also, defining $\mathbf{F_2} = -\mathbf{B_u^T}\mathbf{X_2}$

and $\mathbf{L_2} = -\mathbf{Y_2}\mathbf{C_y^T}$ then the optimal controller is constructed by

$$\mathbf{A_c} = \mathbf{A} + \mathbf{B_u}\mathbf{F_2} + \mathbf{L_2}\mathbf{C_y} \tag{4.19}$$

$$\mathbf{B_c} = -\mathbf{L_2} \tag{4.20}$$

$$\mathbf{C_c} = \mathbf{F_2} \tag{4.21}$$

The solution was based on the following conditions on the open loop plant $\mathbf{G}$

1. $(\mathbf{A}, \mathbf{B_w})$ is stabilizable and $(\mathbf{C_z}, \mathbf{A})$ is detectable
2. $(\mathbf{A}, \mathbf{B_u})$ is stabilizable and $(\mathbf{C_y}, \mathbf{A})$ is detectable
3. $\mathbf{D_{uz}^T}[\mathbf{C_z} \quad \mathbf{D_{uz}}] = [\mathbf{0} \quad \mathbf{I}]$
4. $\begin{bmatrix} \mathbf{B_w} \\ \mathbf{D_{wy}} \end{bmatrix} \mathbf{D_{wy}^T} = \begin{bmatrix} \mathbf{0} \\ \mathbf{I} \end{bmatrix}$

4.3.2 Simulation

A nonlinear simulation of the above was performed using Simulink for $10s$ starting from the following initial states [2]. Two cases were studied, first with a purely transverse load and the second with a combination of transverse and compressive loads.

$$\mathbf{q_0} = [200^\circ, -150^\circ, 60^\circ, 60^\circ, 20^\circ, 30^\circ]^T$$

$$\dot{\mathbf{q}}_\mathbf{0} = [0, 0, 0, 0, 0, 0]^T$$

[2] Simulink block diagram for stabilizing control system shown in Appendix B

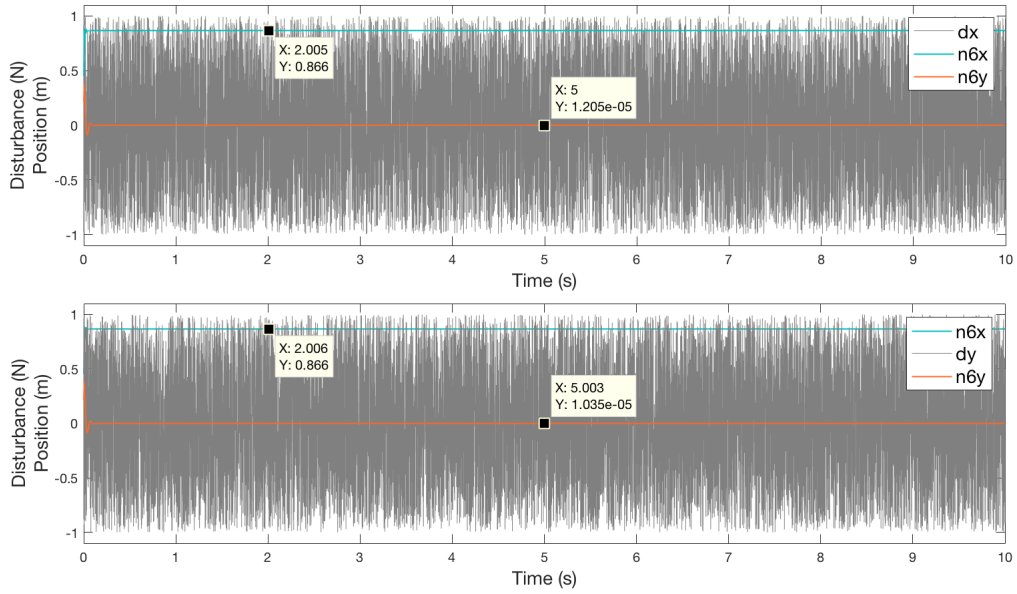

Figure 4.3: Case 1: Random Disturbance Rejection $\mathbf{d} \in [-1, 1]N$

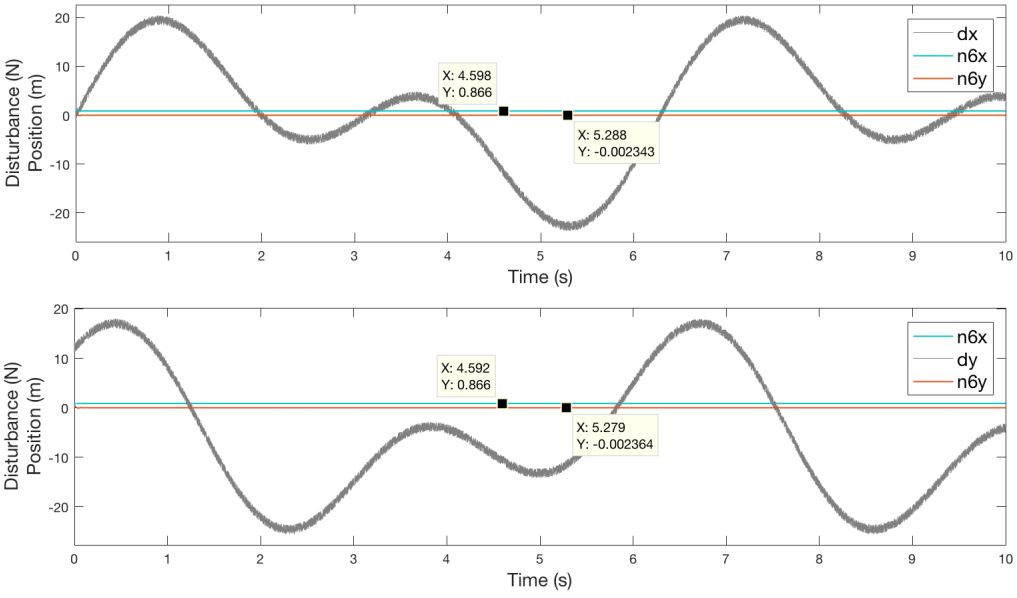

Figure 4.4: Case 1: Sinusoidal Disturbance Rejection $\mathbf{d} \in [-25, 25]N$

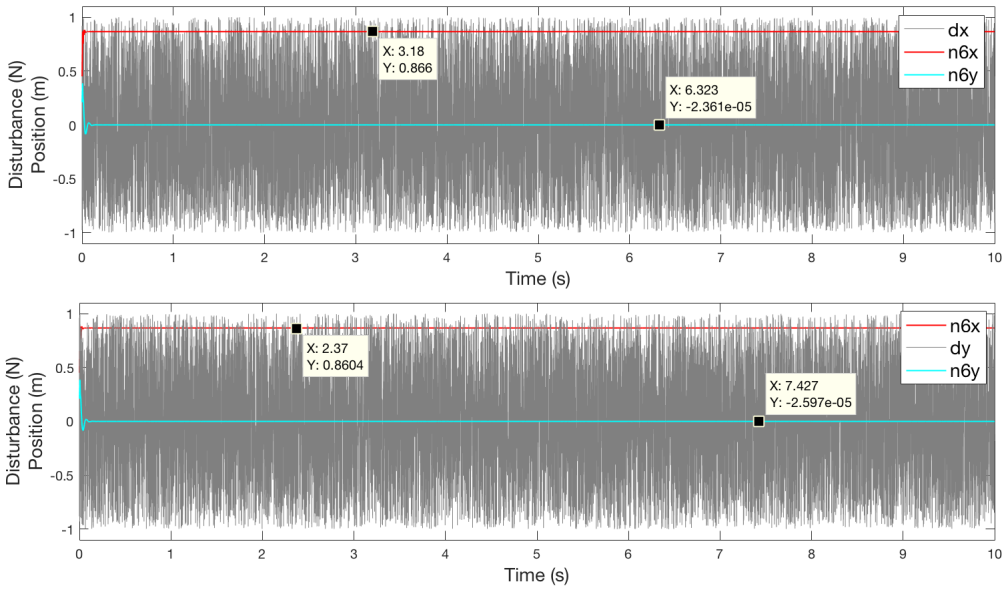

Figure 4.5: Case 2: Random Disturbance Rejection $\mathbf{d} \in [-1, 1]N$

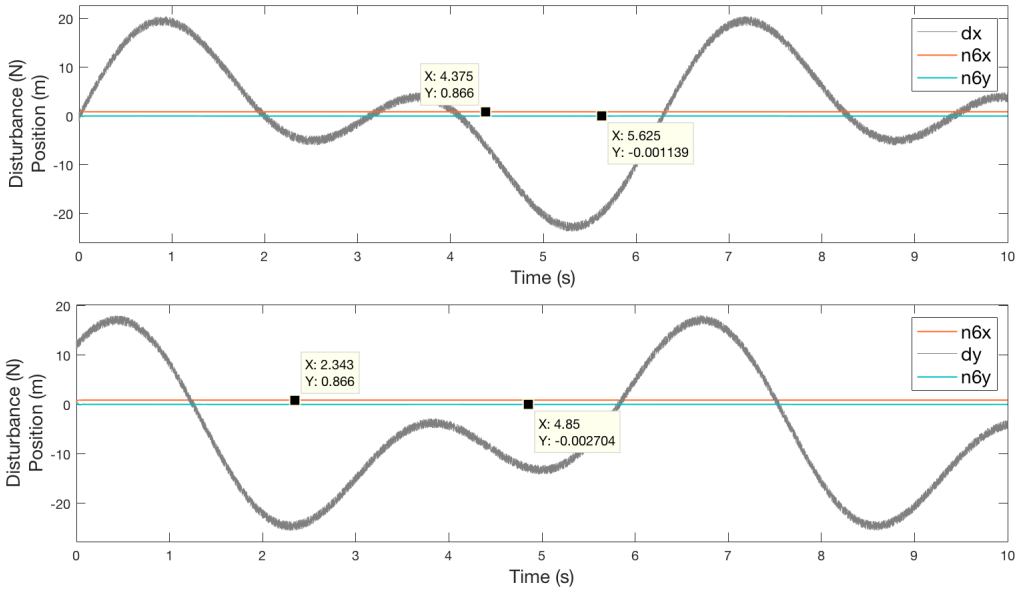

Figure 4.6: Case 2: Sinusoidal Disturbance Rejection $\mathbf{d} \in [-25, 25]N$

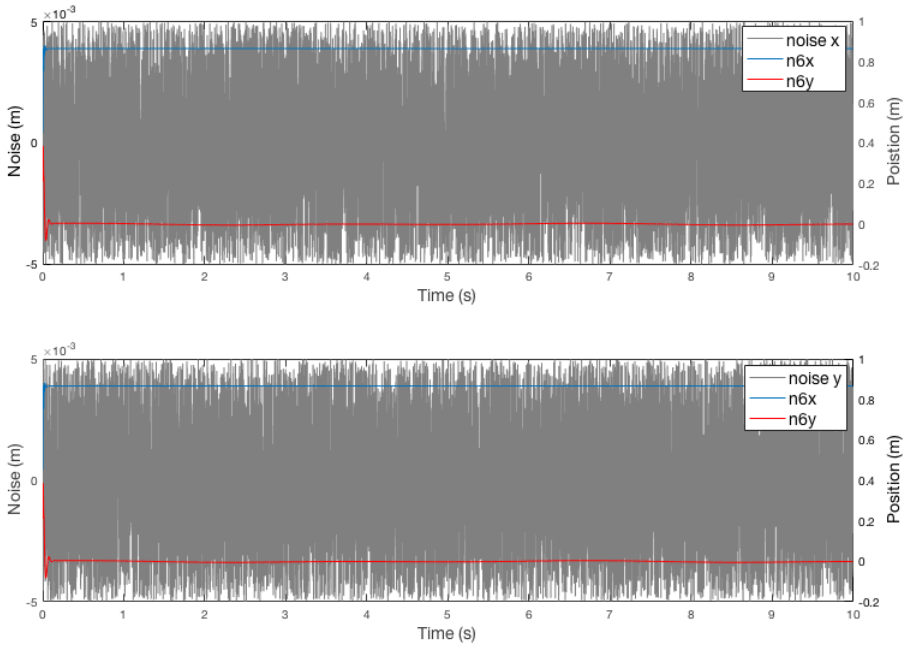

(a) Case 1

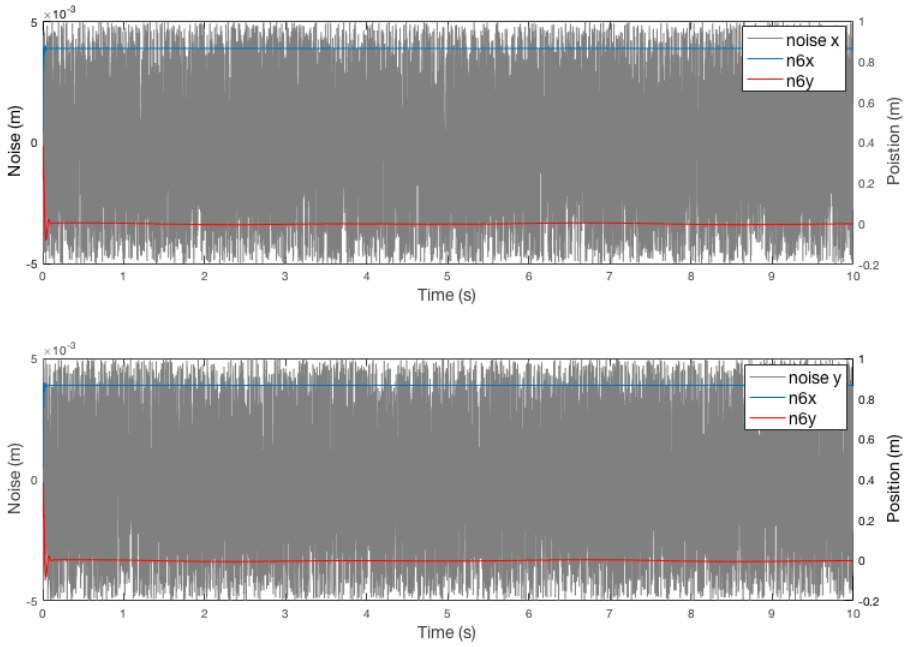

(b) Case 2

Figure 4.7: Noise rejection: Sensor Noise at $\mathbf{n_6} \in [-5, 5]mm$

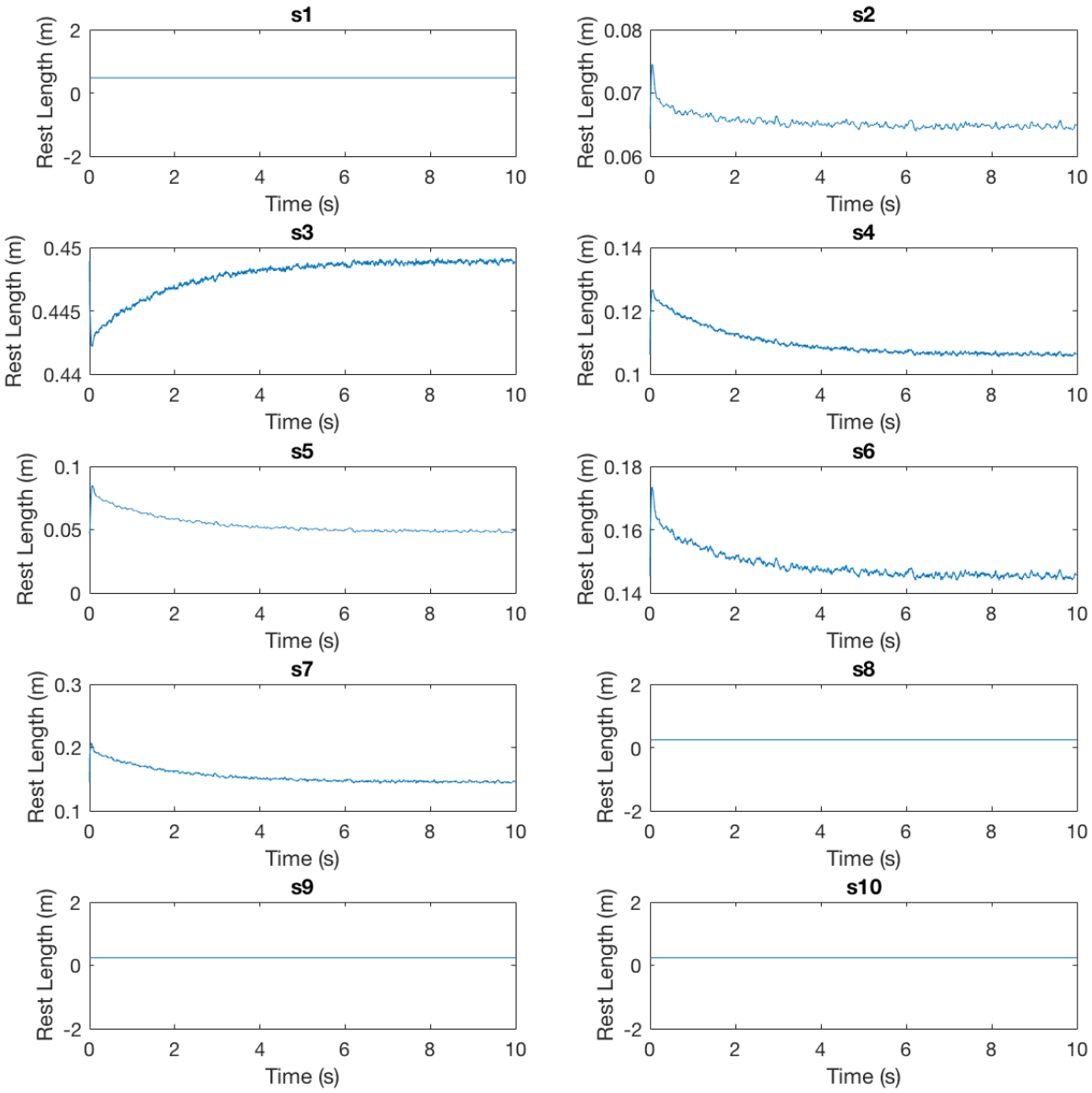

Figure 4.8: Case 2: Control Signals

4.3.2.1 Case 1: Transverse Load

An external load of $[0, -200]N$ was acting in the x, y directions respectively and the coordinates of node $\mathbf{n_6}$ was observed against different disturbances as shown in Fig. (4.3-4.4,4.7). The simulation was performed twice, first using uniform random numbers in $[-1, 1]N$ and then sinusoids in $[-25, 25]N$ as disturbances. In addition, the sensor noise ranged from $[-0.005, 0.005]m$ for each of the sensors. The performance achieved was satisfactory for disturbances as high as $25N$ which was the combined weight of the bars. The H2 optimal cost achieved in this case was

$$||\mathbf{G_{w\to z}}||_2 = 0.0024$$

4.3.2.2 Case 2: Compressive and Transverse Load

An external load of $[-100, -50]N$ was acting in the x, y directions respectively in this case the results are shown in Fig. (4.5-4.7). The disturbances and sensor noise were modeled similar to case 1 and the control signals are presented in Fig. (4.8). The H2 optimal cost achieved was

$$||\mathbf{G_{w\to z}}||_2 = 0.0025$$

4.4 Tracking

The tracking problem involves minimizing error obtained by the difference of the plant's output and a desired signal while simultaneously rejecting disturbance and noise. For the tensegrity robot this relates to tracking a desired trajectory inside its workspace. The goal was to trim the system about an operating point defined in the following equations and enable the controller to guide the position of node $\mathbf{n_6}$ along a given reference signal $\mathbf{r}$.

$$\bar{\mathbf{q}} = [90, -90, 18.2, 18.2, 0, 0]^T \text{ deg}$$

$$\bar{\dot{\mathbf{q}}} = [0, 0, 0, 0, 0, 0]^T \text{ deg/s}$$

$$\bar{\mathbf{d}} = [0, 0]^T \text{ N}$$

$$\bar{\mathbf{u}} = [0.4674, 0.1386, 0.4598, 0.1461, 0.2034, 0.2227, 0.2227, 0.2421, 0.2421, 0.2421]^T \text{ m}$$

4.4.1 H∞ Optimal Control

An H∞ optimal controller was designed to solve the tracking problem [9]. The setup for designing the controller is shown in Fig. (4.7). The plant $\mathbf{G}$ was the linear plant trimmed at the above operating point. The plant had inputs $\mathbf{w}$ (extraneous signals such as disturbance $\mathbf{d} \in \mathbb{R}^{2\times1}$, reference $\mathbf{r} \in \mathbb{R}^{2\times1}$, noise $\mathbf{n} \in \mathbb{R}^{2\times1}$) and $\mathbf{u} \in \mathbb{R}^{10\times1}$ (control). The outputs of the plant were the signals to minimize $\mathbf{z}$ (consisting of the trajectory error $\mathbf{e}$ and control $\mathbf{u}$) and the signal $\mathbf{y_{out}}$. The measured outputs were the position coordinates of the node $\mathbf{n_6}$ denoted by $\mathbf{y} \in \mathbb{R}^{2\times1}$ along with added sensor noise $\mathbf{n}$. The signal $\mathbf{y_{out}}$ was fed back into the controller $\mathbf{K}$ which returned the control $\mathbf{u}$ as output.

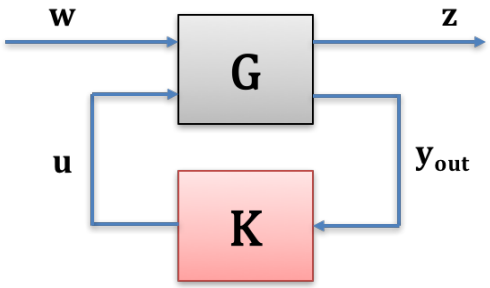

Figure 4.9: Block diagram for H-Infinity control system

The following expressions establish the relationships between the inputs and outputs.

$$\mathbf{e} = W_r\mathbf{r} - \mathbf{y}$$

$$\mathbf{y_m} = \mathbf{y} + W_n\mathbf{n}$$

$$\mathbf{w} = [\mathbf{d}, \mathbf{r}, \mathbf{n}]^T$$

$$\mathbf{z} = [W_e\mathbf{e}, W_u\mathbf{u}]^T$$

$$\mathbf{y_{out}} = [W_r\mathbf{r}, \mathbf{y_m}]^T$$

where

$$W_r = W_e = \begin{bmatrix} \frac{1}{s/5+1} & 0 \\ 0 & \frac{1}{s/5+1} \end{bmatrix}, \quad W_n = 0.0001, \quad W_u = 0.001$$

The weights W_r, W_e, W_n and W_u were multiplied to the respective signals in order to achieve performance goals. The controller [7] was obtained by minimizing the infinity norm of the transfer function $\mathbf{G_{w\to z}}$

$$||\mathbf{G_{w\to z}}||_\infty = sup|\mathbf{G_{w\to z}}| < \gamma$$

subject to the above weights. Defining the Hamiltonian matrices

$$\mathbf{H}_\infty = \begin{bmatrix} \mathbf{A} & \gamma^{-2}\mathbf{B_w}\mathbf{B_w^T} - \mathbf{B_u}\mathbf{B_u^T} \\ -\mathbf{C_z^T}\mathbf{C_z} & -\mathbf{A^T} \end{bmatrix} \qquad \mathbf{J}_\infty = \begin{bmatrix} \mathbf{A^T} & \gamma^{-2}\mathbf{C_z^T}\mathbf{C_z} - \mathbf{C_y^T}\mathbf{C_y} \\ -\mathbf{B_w}\mathbf{B_w^T} & -\mathbf{A} \end{bmatrix}$$

and the Riccatti solutions $\mathbf{X}_\infty = \mathbf{Ric}(\mathbf{H}_\infty)$, $\mathbf{Y}_\infty = \mathbf{Ric}(\mathbf{J}_\infty)$.

Also, defining $\mathbf{F}_\infty = -\mathbf{B_u^T}\mathbf{X}_\infty$, $\mathbf{L}_\infty = -\mathbf{Y}_\infty\mathbf{C_y^T}$ and $\mathbf{Z}_\infty = (\mathbf{I} - \gamma^{-2}\mathbf{Y}_\infty\mathbf{X}_\infty)$ then the optimal controller is constructed by

$$\mathbf{K} = \left[\begin{array}{c|c} \mathbf{A_c} & \mathbf{B_c} \\ \hline \mathbf{C_c} & \mathbf{0} \end{array}\right] \tag{4.22}$$

where

$$\mathbf{A_c} = \mathbf{A} + \gamma^{-2}\mathbf{B_w}\mathbf{B_w^T}\mathbf{X}_\infty + \mathbf{B_u}\mathbf{F}_\infty + \mathbf{Z}_\infty\mathbf{L}_\infty\mathbf{C_y} \tag{4.23}$$

$$\mathbf{B_c} = -\mathbf{Z}_\infty\mathbf{L}_\infty \tag{4.24}$$

$$\mathbf{C_c} = \mathbf{F}_\infty \tag{4.25}$$

The above solution was based on the following conditions on the open loop plant $\mathbf{G}$

1. $(\mathbf{A}, \mathbf{B_w})$ is stabilizable and $(\mathbf{C_z}, \mathbf{A})$ is detectable
2. $(\mathbf{A}, \mathbf{B_u})$ is stabilizable and $(\mathbf{C_y}, \mathbf{A})$ is detectable
3. $\mathbf{D_{uz}^T}[\mathbf{C_z} \quad \mathbf{D_{uz}}] = [\mathbf{0} \quad \mathbf{I}]$
4. $\begin{bmatrix} \mathbf{B_w} \\ \mathbf{D_{wy}} \end{bmatrix} \mathbf{D_{wy}^T} = \begin{bmatrix} \mathbf{0} \\ \mathbf{I} \end{bmatrix}$

4.4.2 Simulation

Linear simulation of the closed loop plant yielded the results shown in Fig. (4.10-4.12). The simulation was performed in MATLAB with a time duration and sample time of $60s$ and $0.001s$ respectively. The disturbances were uniform random numbers ranging from $-20N$ to $20N$ and good disturbance rejection was achieved in both x and y coordinates. The sensor noise varied from $-0.005m$ to $0.005m$ and good noise rejection was achieved. The reference was a sinusoidal signal with an amplitude of 2 and frequency 0.1 rad/s and it was observed that the error signal was minimized against the reference signals in both coordinates.

Nonlinear simulation was also performed in Simulink. The reference signal was sinusoidal in x and y coordinates, representing a circle of diameter $2cm$. The time period of the reference signal was $20s$. In the first case the simulation was performed without disturbance and noise and the results are presented in Fig (4.13-4.16). It was observed that node $\mathbf{n_6}$ tracked the reference signal satisfactorily. However, the errors were profound at the leftmost edge of the circle which was farthest from the operating point, signifying that the dynamics assumed nonlinear behavior in this region.

Next, disturbance ranging from $-2N$ to $2N$ and noise from $-1mm$ to $1mm$ was introduced to the system. It was observed that the tracking performance reduced significantly due to the addition of these extraneous signals. The results are presented in Fig. (4.17). The following optimal cost was achieved

$$||\mathbf{G_{z\rightarrow u}}||_\infty = 0.0039$$

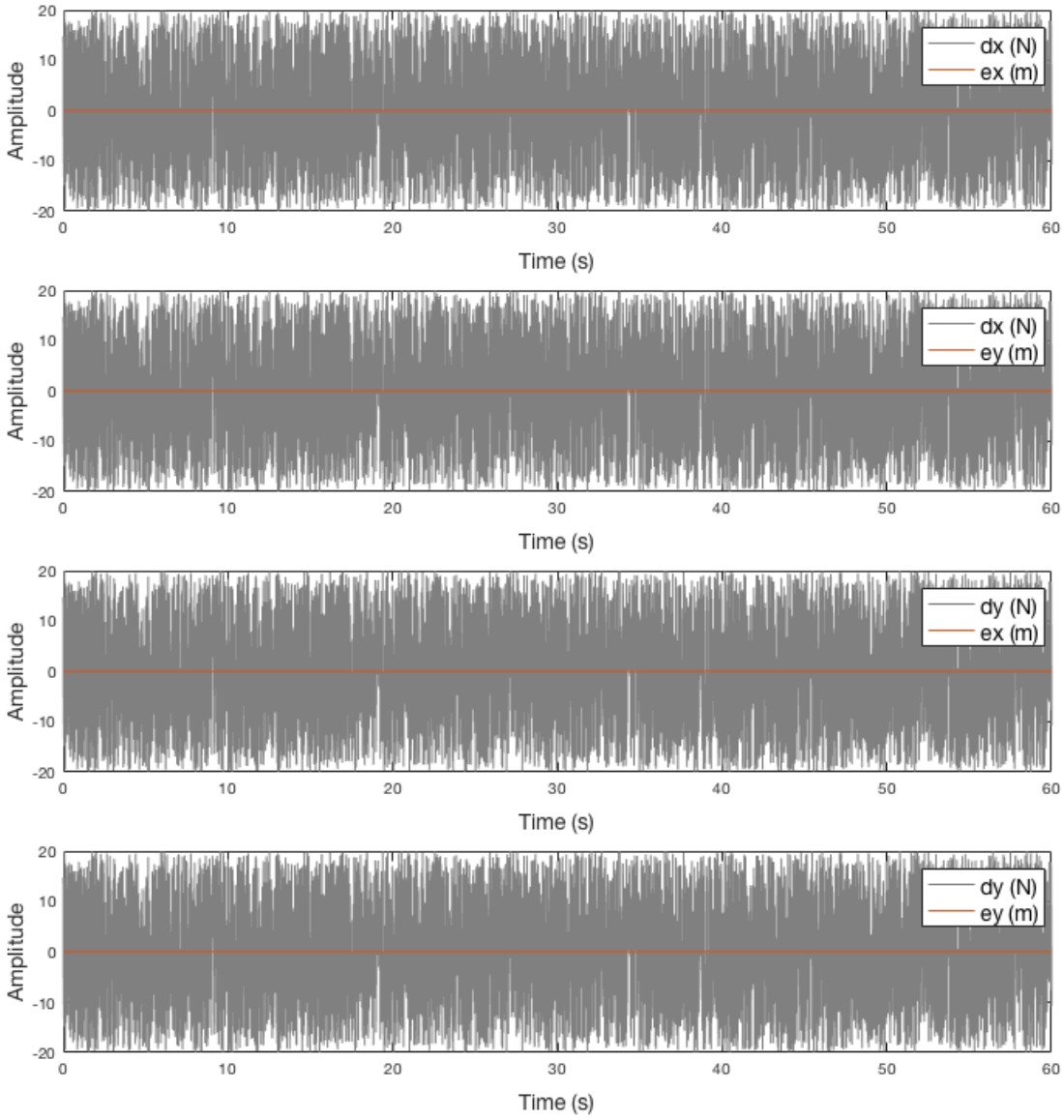

Figure 4.10: Linear sim: Tracking with Disturbance Rejection

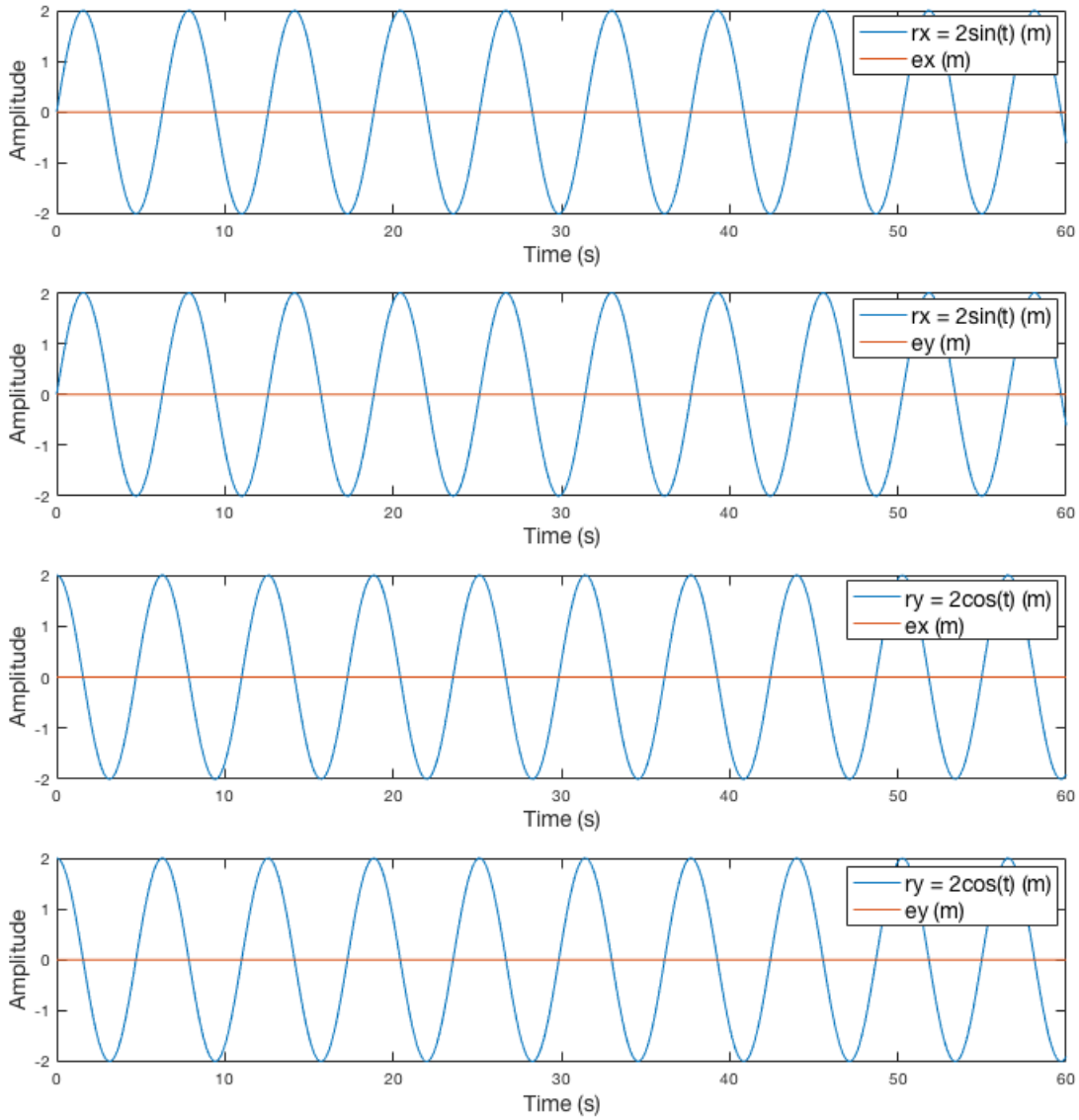

Figure 4.11: Linear sim: Reference vs Error

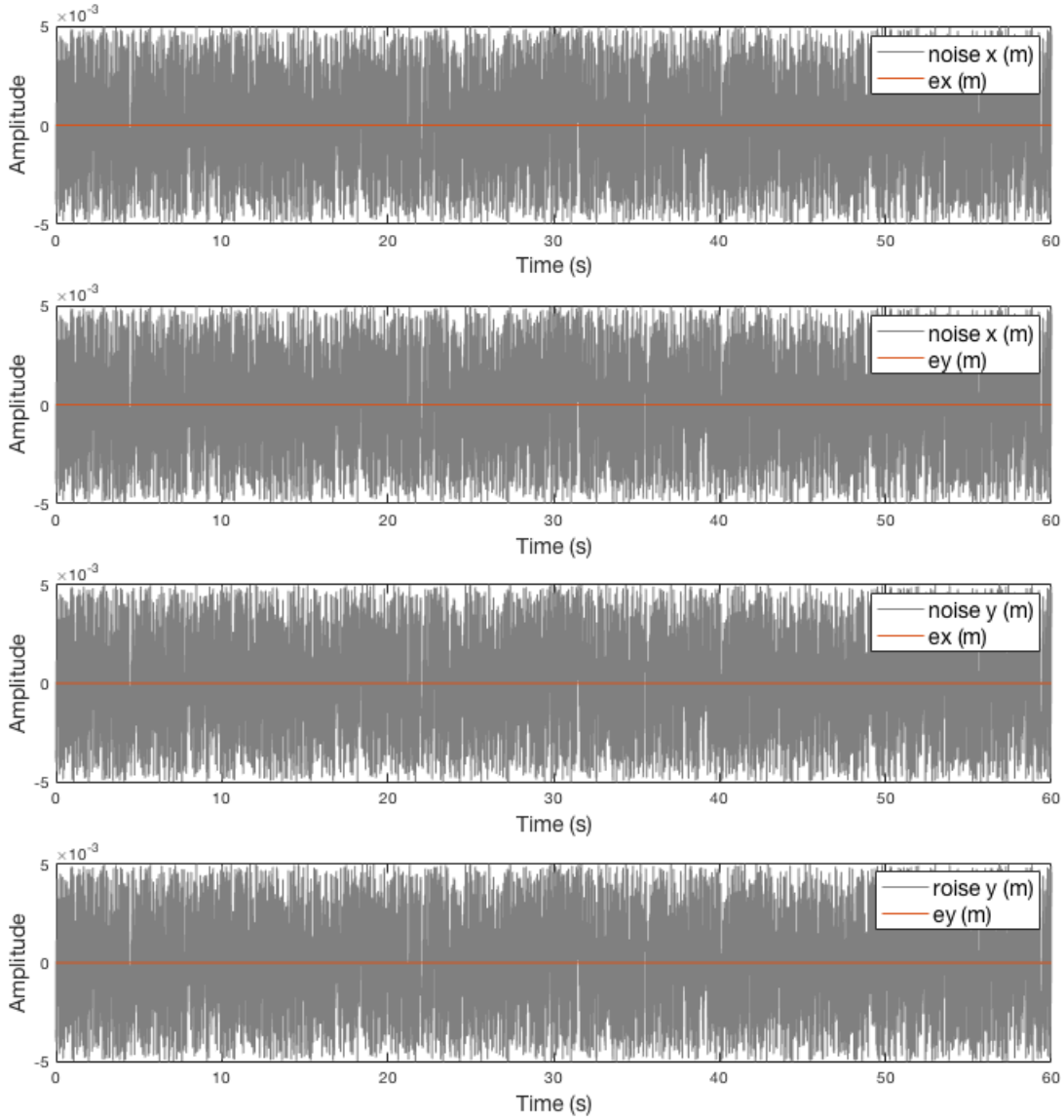

Figure 4.12: Linear sim: Tracking with Noise Rejection

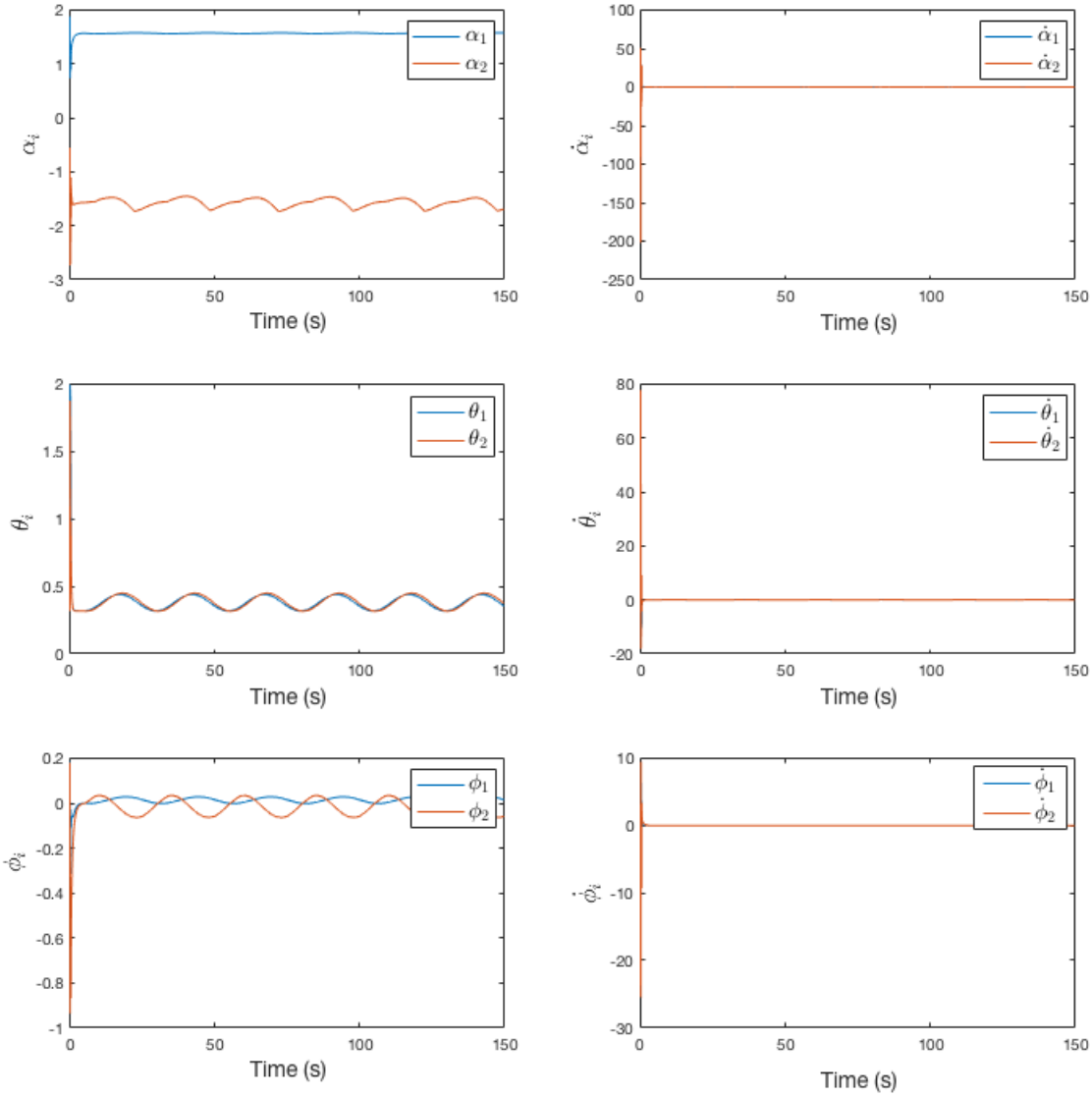

Figure 4.13: Nonlinear tracking sim: Evolution of States

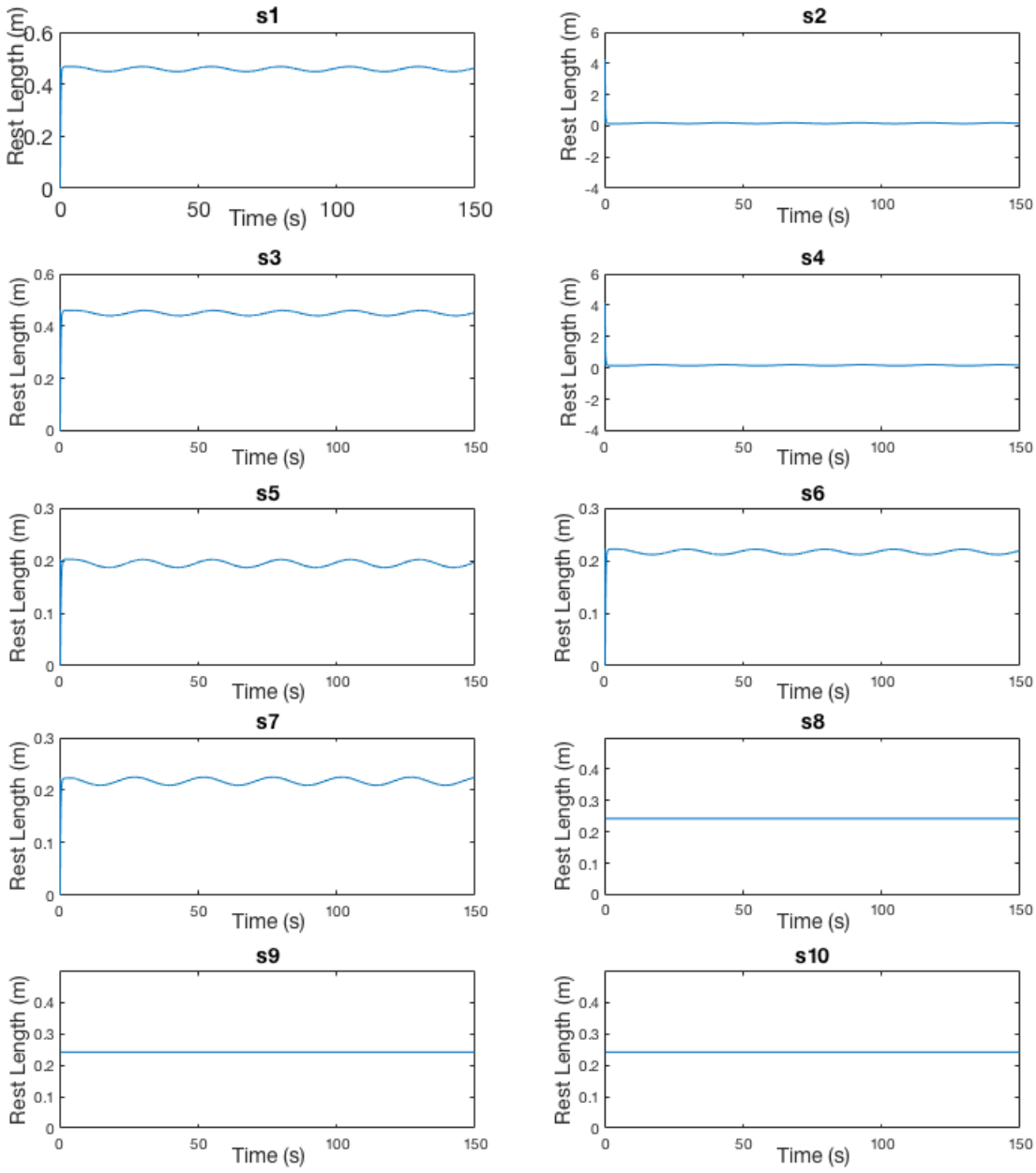

Figure 4.14: Nonlinear tracking sim: Control Signals

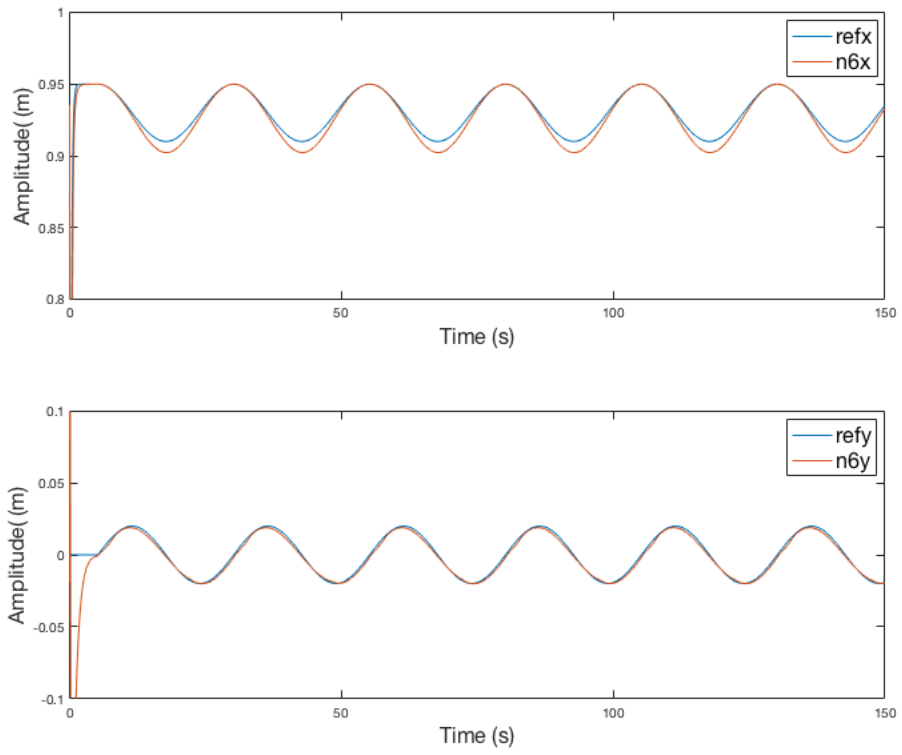

Figure 4.15: Nonlinear tracking sim: Reference vs Output

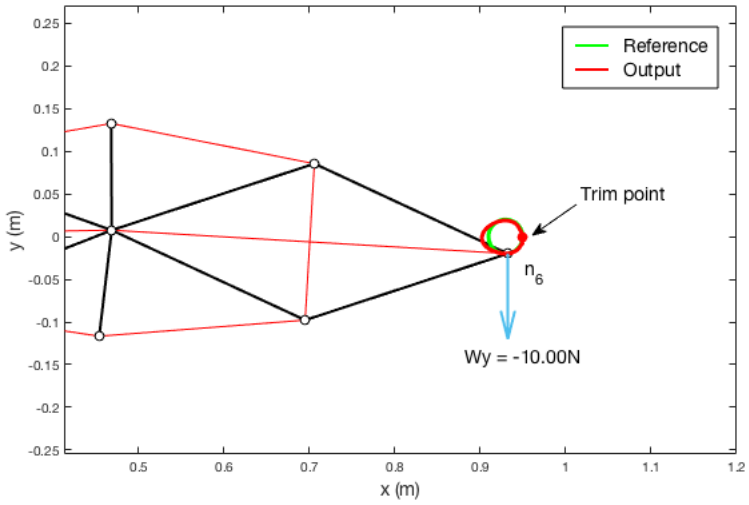

Figure 4.16: Nonlinear tracking sim: Animation Snapshot

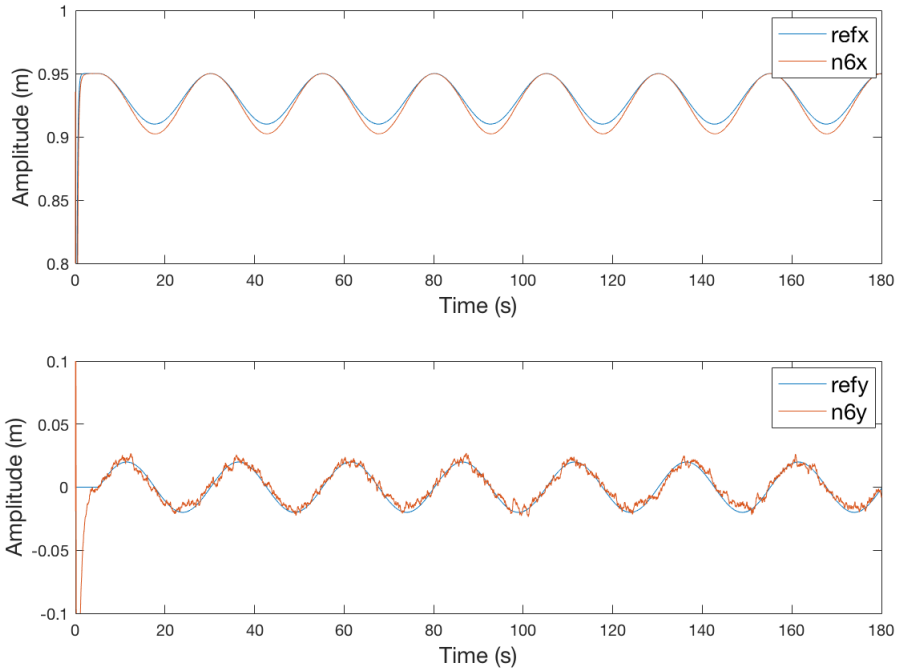

(a) Reference vs output

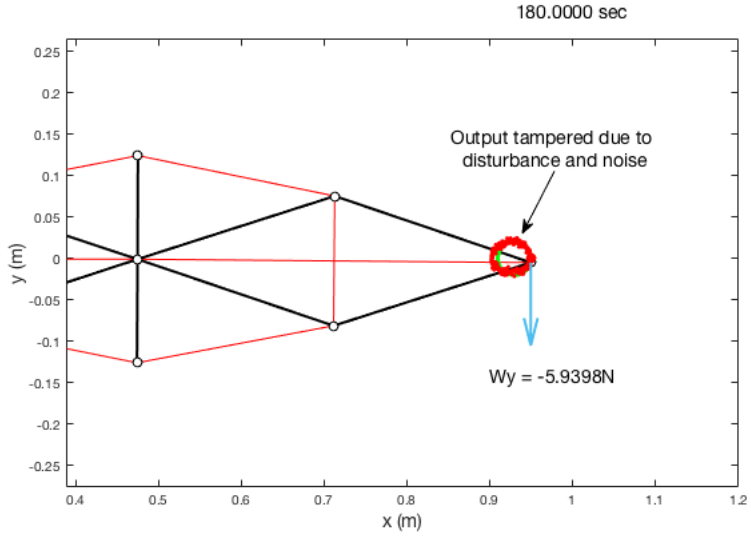

(b) Animation snapshot

Figure 4.17: Nonlinear tracking simulation with disturbance and noise

5. CONCLUDING REMARKS AND FUTURE WORK

The goal of this thesis was to design a tensegrity inspired robot arm with lower mass than a conventional robot arm and to study the dynamics and controls behavior. In Section 2 the tensegrity robot was compared to a load bearing column and a Euler's beam. It was proved that the tensegrity robot design had lower mass for transverse and compressive external loads. This mass minimization was possible because the individual elements in the tensegrity robot experienced pure tension or compression as opposed to other modes of failure.

Section 3 discussed the development of the nonlinear dynamics for the tensegrity structure. The Lagrangian method was chosen because it eliminates the necessity of calculating the constraint forces at the nodes and pinned joints, which was not the focus of this study. The dynamics was developed using minimal coordinates and one downside of doing so is the increase in complexity of the equations as the number of elements in the design increases. Future work could involve the development of the robot dynamics in non-minimal coordinates. However, computational errors at each time-step need to be minimized in such a case.

In Section 4 control problems were solved using Optimal Control theory. The tensegrity structure was stabilized around an operating point in the presence of disturbance and sensor noise. The controller was an optimal design in the H-2 sense and provided sufficient disturbance and noise rejection characteristics. An H∞ controller was also designed to perform robust tracking of a desired trajectory in the presence of disturbance and sensor noise.

Future work on this robot could be dedicated towards building a prototype. The selection of actuators within the frequency range of the control signals is also an

important design criteria and a review of existing actuator technology needs to be performed. The study could also be combined with implementing an optimal sensing architecture that could minimize the amount of actuation in the system. Other areas for extending this work could be studying the feasibility of using piezoelectric actuators for actuating the strings, or replacing the steel strings by piezoelectric strings.

REFERENCES

[1] R. E. Skelton and M. de Oliveira, *Tensegrity Systems*. Springer US, 1 ed., 2009.

[2] R. B. Fuller, "Tensegrity," *Portfolio and Art News Annual*, vol. 4, pp. 112–127, 1961.

[3] S. Pellegrino, "Structural computations with the singular value decomposition of the equilibrium matrix," *In. Journal of Solids and Structures*, vol. 30, pp. 3025–3025, 1993.

[4] S. Guest, "The stiffness of prestressed frameworks: A unifying approach," *International Journal of Solids and Structures*, vol. 43, pp. 842–854, 2006.

[5] K. Nagase and R. Skelton, "Minimal mass design of tensegrity structures," in *Proceedings of SPIE - The International Society for Optical Engineering*, vol. 9061, 03 2014.

[6] J. Cheong and R. Skelton, "Nonminimal dynamics of general class k tensegrity systems," *International Journal of Structural Stability and Dynamics*, vol. 15, p. 1450042, 03 2015.

[7] J. C. Doyle, K. Glover, P. P. Khargonekar, and B. A. Francis, "State-space solutions to standard h2 and h infin; control problems," *IEEE Transactions on Automatic Control*, vol. 34, no. 8, pp. 831–847, 1989.

[8] R. Bhattacharya, "Tensegrity multibody report," tech. rep., Texas A&M University, 2017.

[9] R. Bhattacharya, "Lecture notes on design of advanced flight control systems," tech. rep., Texas A&M University.

APPENDIX A

ROBOT GEOMETRY

A.1 Expressions for Nodes

The simple 3-rotation matrix (rotation about z-axis by angle ψ) is defined by

$$C(\psi) = \begin{bmatrix} \cos\psi & -\sin\psi & 0 \\ \sin\psi & \cos\psi & 0 \\ 0 & 0 & 1 \end{bmatrix} \tag{A.1}$$

The nodes are given by

$$\mathbf{n_1} = [0, 0, 0]^T \tag{A.2}$$

$$\mathbf{n_2} = \mathbf{n_1} + C(\phi_1)C(\theta_1)[L_d, 0, 0]^T \tag{A.3}$$

$$\mathbf{n_3} = \mathbf{n_2} + C(\phi_1)C(-\theta_1)[L_d, 0, 0]^T \tag{A.4}$$

$$\mathbf{n_4} = \mathbf{n_1} + C(\phi_1)C(-\theta_1)[L_d, 0, 0]^T \tag{A.5}$$

$$\mathbf{n_5} = \mathbf{n_3} + C(\phi_2)C(\theta_2)[L_d, 0, 0]^T \tag{A.6}$$

$$\mathbf{n_6} = \mathbf{n_5} + C(\phi_2)C(-\theta_2)[L_d, 0, 0]^T \tag{A.7}$$

$$\mathbf{n_7} = \mathbf{n_3} + C(\phi_2)C(-\theta_2)[L_d, 0, 0]^T \tag{A.8}$$

$$\mathbf{n_8} = \mathbf{n_3} + C(\alpha_1)[L_t, 0, 0]^T \tag{A.9}$$

$$\mathbf{n_9} = \mathbf{n_3} + C(\alpha_2)[L_t, 0, 0]^T \tag{A.10}$$

$$\mathbf{n_{10}} = \mathbf{n_1} + [0, L_t, 0]^T \tag{A.11}$$

$$\mathbf{n_{11}} = \mathbf{n_1} + [0, -L_t, 0]^T \tag{A.12}$$

A.2 Expressions for Angular Velocities

The angular velocities of the bars are given by

$$\omega_{\mathbf{1}} = [0, 0, \dot{\theta}_1 + \dot{\phi}_1] \tag{A.13}$$

$$\omega_{\mathbf{2}} = [0, 0, -\dot{\theta}_1 + \dot{\phi}_1] \tag{A.14}$$

$$\omega_{\mathbf{3}} = [0, 0, -\dot{\theta}_1 + \dot{\phi}_1] \tag{A.15}$$

$$\omega_{\mathbf{4}} = [0, 0, \dot{\theta}_1 + \dot{\phi}_1] \tag{A.16}$$

$$\omega_{\mathbf{5}} = [0, 0, \dot{\theta}_2 + \dot{\phi}_2] \tag{A.17}$$

$$\omega_{\mathbf{6}} = [0, 0, -\dot{\theta}_2 + \dot{\phi}_2] \tag{A.18}$$

$$\omega_{\mathbf{7}} = [0, 0, -\dot{\theta}_2 + \dot{\phi}_2] \tag{A.19}$$

$$\omega_{\mathbf{8}} = [0, 0, \dot{\theta}_2 + \dot{\phi}_2] \tag{A.20}$$

$$\omega_{\mathbf{9}} = [0, 0, \dot{\alpha}_1] \tag{A.21}$$

$$\omega_{\mathbf{10}} = [0, 0, \dot{\alpha}_2] \tag{A.22}$$

APPENDIX B

SIMULINK BLOCK DIAGRAMS

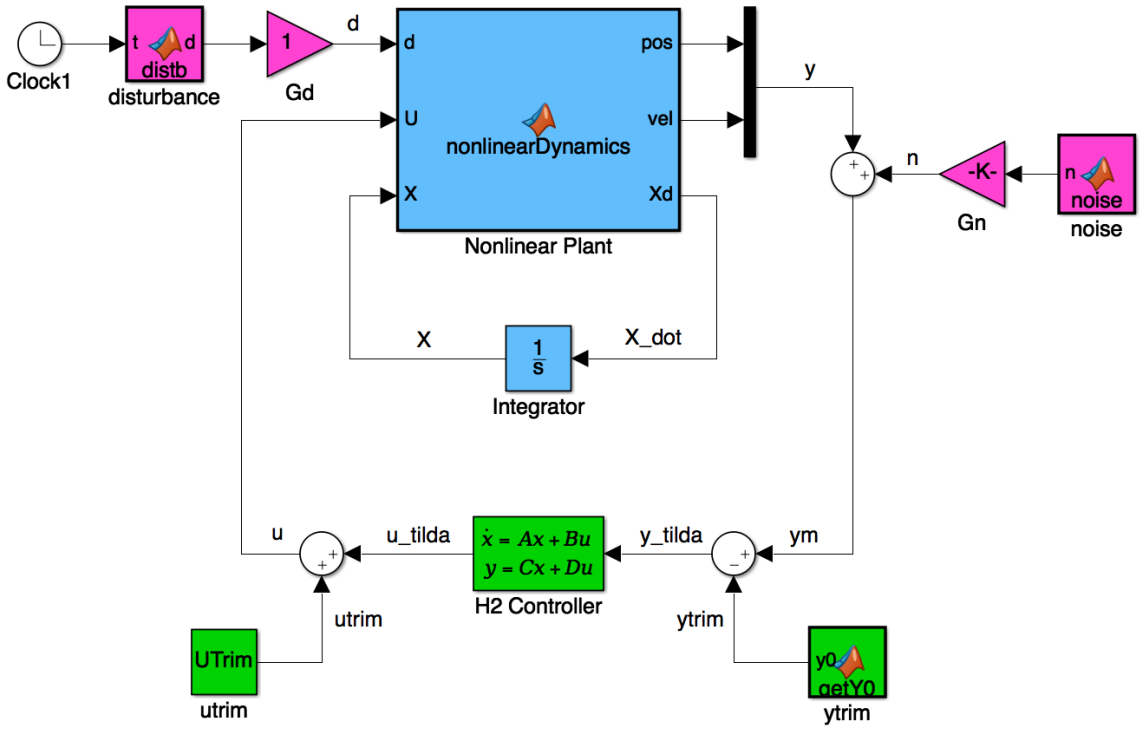

Figure B.1: Simulink block diagram for stabilization problem

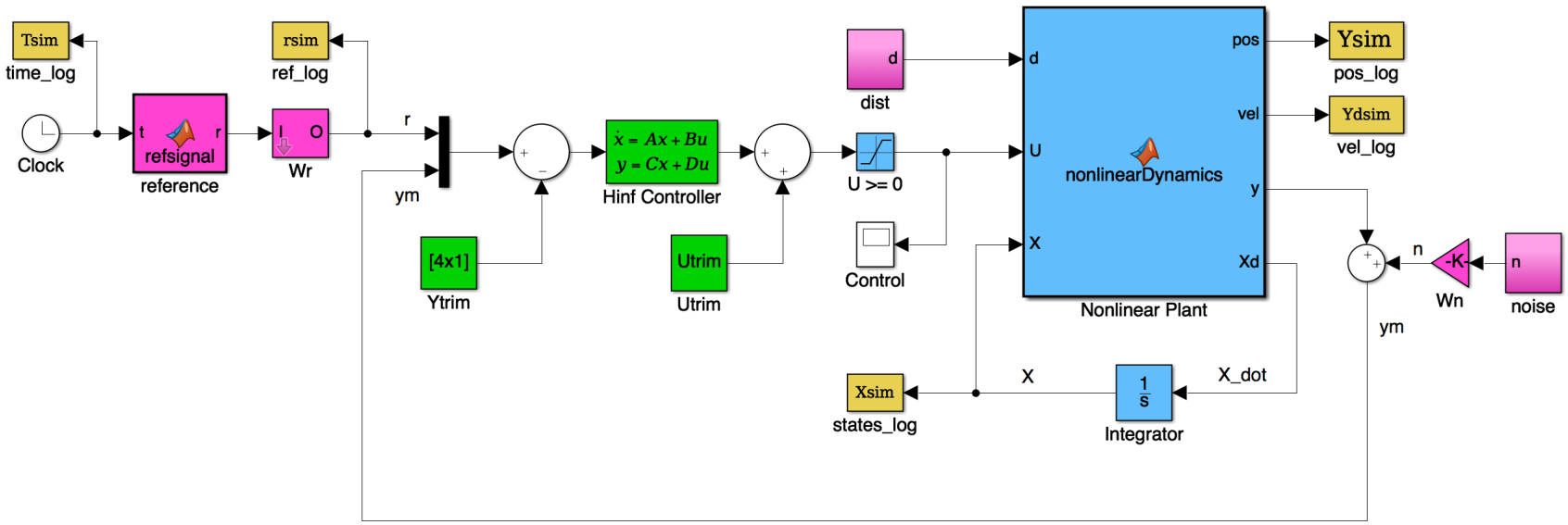

Figure B.2: Simulink block diagram for tracking problem